UNIVERSITY OF CALIFORNIA SAN DIEGO

The role of F-box protein FBXA-11 in regulating thermotolerance in *Caenorhabditis elegans*

A Thesis submitted in partial satisfaction of the requirements
for the degree Master of Science

in

Biology

by

Yingyin Li

Committee in charge:

Professor Emily Troemel, Chair
Professor Christina Hueschen
Professor Amy Pasquinelli

2024

The Thesis of Yingyin Li is approved, and it is acceptable in quality and form for publication on microfilm and electronically.

University of California San Diego

2024

TABLE OF CONTENTS

LIST OF FIGURES

LIST OF TABLES

ACKNOWLEDGEMENTS

I would like to extend my heartfelt gratitude to the many people who have supported me through the completion of this thesis.

To my supervisor, Dr. Emily Troemel, thank you for your patience and guidance throughout my research journey. Your advice and assistance have been truly valuable for my personal and professional growth throughout this program and during all the years. To my mentors, Mario and Nicole, thank you for always being by my side and always so willing to share your knowledge and skills. I am truly grateful for all the encouragement and support you have provided me on so many different fronts. To all the past and the present Troemel Lab members that I had the pleasure to work with, thank you for all the scientific support, discussion and friendship; I could not have asked for better colleagues and friends.

Finally, to my family, thank you for your love, encouragement, and support through all the ups and downs. I could not have done this without you.

ABSTRACT OF THE THESIS

The role of F-box protein FBXA-11 in regulating thermotolerance in *Caenorhabditis elegans*

by

Yingyin Li

Master of Science in Biology

University of California San Diego, 2024

Professor Emily Troemel, Chair

In the nematode *Caenorhabditis elegans*, a stress/immune response pathway called the Intracellular Pathogen Response (IPR) increases resistance to proteotoxic stress. In mutants with constitutive IPR activation, a CUL-6 cullin-RING ubiquitin ligase complex was previously shown to protect the host from heat shock. This complex recently was found to target a putative substrate, the molecular chaperone HSP-90, leading to its degradation to improve resistance to

heat shock (thermotolerance), as a readout for proteostasis. However, which F-box proteins might be involved in targeting HSP-90 was unclear. Here I assessed the role of an F-box protein, FBXA-11, using *fbxa-11* RNAi, an *fbxa-11* partial deletion mutant, and a null allele mutant *fbxa-11(jy194)* that I generated via CRISPR-Cas9-mediated genome editing. My results demonstrated differing effects of *fbxa-11* RNAi on thermotolerance compared to *fbxa-11* mutants. Preliminarily, I found that *fbxa-11* RNAi does not affect thermotolerance in *fbxa-11* mutants, suggesting the discrepancy is this case may not be due to off-target effects, but rather due to compensatory increased thermotolerance in *fbxa-11* mutants. These findings are consistent with a model that wild-type *fbxa-11* promotes thermotolerance. Also consistent with this model, I found that *fbxa-11(jy194)* suppresses the increased thermotolerance caused by overexpression of CUL-6. Through examining the effects on HSP-90 levels upon *fbxa-11* RNAi and *fbxa-11* mutations, I found mixed results indicating there may be off-target effects of *fbxa-11* RNAi in this context. I also found that the CUL-6 ubiquitin ligase complex likely targets substrates in addition to HSP-90 to promote thermotolerance. In conclusion, we identified FBXA-11 as a new F-box adapter protein potentially acting in a CUL-6 ubiquitin ligase complex to improve thermotolerance as part of the IPR, furthering our understanding of how *C. elegans* copes with proteotoxic stress.

INTRODUCTION

Maintaining protein homeostasis (proteostasis) is important for safeguarding cellular protein quality and organismal health. A diverse series of regulatory cellular pathways work as part of the proteostasis network to provide protection against proteotoxic stressors that cause protein damage, aggregation, and misfolding (Powers et al., 2009). The resulting proteotoxicity as this damage accumulates can impact normal cellular and organellar function, and is associated with the development of cancers, neurodegenerative diseases, age-related pathologies, and inflammation (Ho Zhi Guang et al., 2019; Kettern et al., 2010; Morimoto, 2008; Ruano, 2021). Stressors that disrupt proteome integrity and contribute to proteotoxicity are diverse and can include abnormal pH, oxidative stress, temperature, as well as pathogen infection (Aviner & Frydman, 2020; Willis & Patterson, 2013).

Intracellular pathogens in particular can cause proteotoxicity to host cells during their invasion, replication and maturation inside these cells. To battle the impacts of proteotoxic stress, diverse host response factors serve to maintain proteostasis, including molecular chaperones for refolding misfolded or denatured proteins, as well as the ubiquitin system that conjugates the small protein ubiquitin onto substrates to alter their fates, usually for degradation (Ciechanover, 1998; Ellis & Vies, 1991; To et al., 2022). These proteostasis systems can be severely burdened by intracellular pathogens. For instance, viruses use host factors such as chaperones to fold their own proteins, which then limits the capacity of chaperones to fold host proteins. Viruses also commonly suppress and/or hijack host translation machinery, which then reduces the levels of host protein synthesis. Altogether these and other pathogen strategies that are designed to facilitate pathogen growth can lead to dysregulation of the host proteostasis network, together

with the increased demands on proteostasis caused by immune responses (Aviner & Frydman, 2020).

In addition to viruses, several other types of pathogens can disrupt host proteostasis. For example, the microsporidian species *Nematocida parisii* (*N. parisii*), which is an obligate intracellular pathogen naturally infecting the model nematode *C. elegans*, disrupts proteostasis as it progresses through its life cycle inside the intestine. In particular during later stages of *N. parisii* infection, host intestinal cells exhibit clusters of ubiquitin aggregates, which are a hallmark of proteotoxic stress (Bakowski et al., 2014). Many studies in *C. elegans* as well as other hosts have shown that ubiquitylation has a role in conferring protection against infection, including ubiquitylation of invading intracellular pathogens such as microsporidia and the Orsay virus to potentially target them for degradation through autophagy (Bakowski et al., 2014; Balla et al., 2019). Host targeting of intracellular bacteria has also been shown in many systems; for example, the pathogen *M. tuberculosis* can be recognized by the ubiquitin-recognition receptors that facilitates interaction with autophagy proteins and their subsequent degradation (Kuo et al., 2018). Indeed, ubiquitin-mediated degradation pathways are often involved in battles between hosts and pathogens (Lažetić, 2020; Mello-Vieira et al., 2023).

Recently, a proteostasis/immune response pathway known as the Intracellular Pathogen Response (IPR) was discovered in the *C. elegans*, which involves upregulation of several ubiquitin ligase components. This pathway is activated by natural intracellular pathogen infection by *N. parisii* and the Orsay virus, as well as by proteotoxic stress including chronic heat stress (30°C for 24 hours) and blockade of the proteasome. The IPR functions to increase resistance to intracellular infection, as well as tolerance of perturbations to proteostasis, such as

exposure to heat shock (Bakowski et al., 2014; Panek et al., 2020; Reddy et al., 2017, 2019). Induction of the IPR is modulated by members of the *pals* (protein containing ALS2CR12) gene family, which encode for proteins with unknown biochemical functions. The *pals* gene family is expanded in *C. elegans* genome, containing 39 *pals* genes, compared to just 1 *pals* gene in humans (Reddy et al., 2019). In *C. elegans, pals-22* is a negative regulator of the IPR, which constrains the activity of *pals-25,* which is an activator of the IPR (Reddy et al., 2019). *pals-22* mutants have several phenotypes including constitutively upregulated IPR genes, increased resistance to infection, and increased resistance to heat shock, aka thermotolerance. All of these phenotypes are reversed to wild-type levels in *pals-22 pals-25* double mutants.

IPR genes include several genes that encode components of a recently defined cullin-ring ubiquitin ligase complex that promotes thermotolerance (Panek et al., 2020; Figure 1A). Cullin-ring ubiquitin ligases (CRLs) are the largest class of E3 ubiquitin ligases, which are enzymes that conjugate a ubiquitin tag onto substrates. A subset of CRLs include the SCF (Skp-Cullin-F-box) ligases, which are comprised of three core components (a RING domain protein, an s-phase kinase associated protein SKP, and a cullin protein) plus an F-box protein, which identifies the target for ubiquitylation and provides specificity to the ubiquitin ligase complex (Yen & Elledge, 2008). F-box proteins contain an F-box domain at the N terminus, which is defined as a 42-48 amino acid motif allowing for direct binding with SKP during SCF ligase assembly (Ma et al., 2021). At the C-terminus of the protein is the more variable substrate-binding domain that confers specificity for the diverse substrates of SCF ligases. The *C. elegans* genome contains a greatly expanded F-box repertoire, likely as a result of positive selection, with up to 520 F-box

genes being present in the genome, although very few of them have assigned functions (Ma et al., 2021; Thomas, 2006).

The Troemel lab has characterized F-box proteins and other components of an SCF ubiquitin ligase complex that promotes thermotolerance as part of the IPR. First, in a *pals-22* loss of function mutant background where the IPR is constitutively activated, we found that the SCF core component cullin protein CUL-6 is required for the increased thermotolerance of *pals-22* mutants (Reddy et al., 2017). Then, using a transgenic strain with an overexpression of CUL-6 in the intestine (hereafter referred to as CUL-$6^{int\text{-}OE}$), we found that CUL-6 overexpression alone could mimic the *pals-22* phenotype of improving thermotolerance. Through coimmunoprecipitation-mass spectrometry (co-IP/MS) and genetic analyses, we defined other components of a ubiquitin ligase complex acting with CUL-6 to promote thermotolerance. Specifically, we found CUL-6 acts with a previously uncharacterized RING domain protein that was named RCS-1 (potentially acting in lieu of RBX). We also found CUL-6 acts with three SKP-related proteins SKR-3, SKR-4, and SKR-5 acting redundantly, as well as with two F-box proteins FBXA-75 and FBXA-158 acting non-redundantly. Specifically, FBXA-75 and FBXA-158 were each required for promoting thermotolerance in *pals-22* loss of function mutants, as well as in a CUL-6 overexpression background (Panek et al., 2020; Figure 1A, B, C). Given the redundancy of SKR-3, SKR-4 and SKR-5, together with the requirement for two separate F-box proteins, this CUL-6 ubiquitin ligase complex is likely to be a complicated multimer, potentially comprised of two or more distinct tetramers and/or a heterodimer of two or more tetramers.

Recent findings have demonstrated that the large heat shock protein HSP-90 is a candidate substrate for ubiquitylation by the CUL-6 ubiquitin ligase, as part of a model whereby a CUL-6 ubiquitin ligase directs HSP-90 to intestinal lysosomes and/or lysosome-related organelles for degradation, to ultimately promote thermotolerance (Bardan Sarmiento et al., 2024). These findings are somewhat surprising, because HSP-90 is generally thought to promote thermotolerance as a foldase that interacts with diverse client proteins to promote proteostasis by assisting in their protein folding and preventing cytotoxic protein aggregates (Schopf et al., 2017). However, several findings indicate that in some contexts, HSP-90 can actually impair thermotolerance. Specifically, in *C. elegans*, loss of HSP-90 will increase survival after heat shock, and overexpression of HSP-90 will decrease survival upon heat shock (Bardan Sarmiento et al., 2024). Although it has not been demonstrated that the CUL-6 ubiquitin ligase directly targets HSP-90 for ubiquitylation, several lines of evidence indicate CUL-6 ubiquitin ligase activity causes HSP-90 degradation to promote thermotolerance. Specifically, when HSP-90 is overexpressed, loss of CUL-6 will decrease thermotolerance, and when CUL-6 is overexpressed, it will increase thermotolerance (Bardan Sarmiento et al., 2024; Figure 2A, B). Furthermore, loss of CUL-6 causes increased levels of HSP-90::RFP expression driven from an intestinal specific promoter *vha-6* (hereafter referred to as HSP-90::RFP$^{int\text{-}OE}$), and overexpression of CUL-6 causes decreased levels of HSP-90::RFP$^{int\text{-}OE}$. In both of these cases, the effects are dependent on CUL-6 neddylation, which is a post-translational modification of cullins that involves the attachment of ubiquitin-like protein NEDD8 onto a conserved lysine residue on the cullin protein, to promote ubiquitin ligase activity (Duda et al., 2008). Although CUL-6 was shown to regulate HSP-90 levels and direct its subsequent targeting to lysosomes to promote thermotolerance, the other components acting in a CUL-6 ubiquitin ligase complex to target

HSP-90 were not clear. In particular, the F-box proteins working with CUL-6 in this context were unknown.

Given that F-box proteins FBXA-75 and FBXA-158 were found to be in a physical complex with CUL-6 protein, and that they each were required to promote thermotolerance in *pals-22* mutants where CUL-6 is upregulated, their role with HSP-90 was investigated by Troemel lab manager, Mario Bardan Sarmiento. If FBXA-75 and -158 were acting with CUL-6 to target HSP-90 for degradation, then loss of these proteins in the HSP-90::RFP$^{int\text{-}OE}$ background would be expected to have the same phenotype as loss of CUL-6; i.e. their loss should lead to decreased thermotolerance and increased levels of HSP-90. However, Mr. Bardan Sarmiento found that knockout of *fbxa-75* in the HSP-90::RFP$^{int\text{-}OE}$ background increased thermotolerance, and had no effect on HSP-90::RFP levels (unpublished, Bardan Sarmiento; Figure 3A). Furthermore, it was found that while knockout of *fbxa-158* in the HSP-90::RFP$^{int\text{-}OE}$ background decreased thermotolerance, it did not further increase HSP-90::RFP levels (unpublished, Bardan Sarmiento; Figure 3A, B). Given these results, FBXA-75 and FBXA-158 seemed unlikely to be working with CUL-6 to degrade HSP-90 and promote thermotolerance.

Here, we investigated which F-box protein(s) might acting in a CUL-6/cullin ubiquitin ligase to target HSP-90 for degradation to promote thermotolerance. In the prior co-IP/MS study to identify CUL-6 interactors, three F-box proteins were identified in addition to FBXA-75 and FBXA-158. Specifically, FBXA-11, FBXA-54, FBXA-188 were all identified as candidate CUL-6 interactors, although they were below the cut-off level for statistical significance (Panek et al., 2020). To test their role in thermotolerance and controlling HSP-90 degradation, Mr.

Bardan Sarmiento performed RNAi against these three genes, and found that RNAi knockdown of *fbxa-11* decreased thermotolerance and increased the level of HSP-90::RFP, although the latter was not quantified (Figure 3C, 4A). These findings supported a model that FBXA-11 might act in a CUL-6 ubiquitin ligase complex to target HSP-90 for degradation to improve thermotolerance.

To better understand the role of *fbxa-11*, I performed additional *fbxa-11* RNAi experiments, characterized an existing *fbxa-11* partial deletion mutant, and also generated a *fbxa-11* full deletion via CRISPR-Cas9-mediated genome editing and characterized this mutant. From these analyses, I found both the partial deletion and full deletion *fbxa-11* mutants had increased thermotolerance in an HSP-90::RFP$^{int\text{-}OE}$ background. These results are distinct from those we found with *fbxa-11* RNAi, which caused decreased thermotolerance in an HSP-90::RFP$^{int\text{-}OE}$ background. Importantly, I found in preliminary experiments that *fbxa-11* RNAi no longer decreased thermotolerance in the full deletion *fbxa-11(jy194)* mutant I created, indicating that the discrepancy between the thermotolerance phenotypes of *fbxa-11* RNAi and *fbxa-11(jy194)* mutants may not be due to off-target effects from RNAi in this context. Instead, these results suggest there may be some form of compensation occurring in *fbxa-11* mutants that causes the opposite phenotype as *fbxa-11* RNAi. These results, together with my other findings described below, demonstrate that there are intriguing differences between RNAi and mutant analysis for F-box genes in thermotolerance, as well as strain background-specific effects. Altogether my studies provide new insights about regulation of proteostasis by F-box genes, highlighting exciting next steps to better understand how this greatly expanded gene family helps *C. elegans* cope with proteotoxic stress.

Figure 1: F-box proteins FBXA-75 and FBXA-158 are required to promote thermotolerance in a *pals-22* mutant background and a CUL-6 overexpression background, but not in a wild-type background.

A) A model of the CUL-6 ubiquitin ligase complex promoting thermotolerance as part of the IPR in a *pals-22* mutant background. The IPR includes transcriptional upregulation of components of a CUL-6 SKP/Cullin/F-box (SCF) E3 ubiquitin ligase. CUL-6 act with other ubiquitin ligase subunits including Skp-related proteins SKR-3, SKR-4, and SKR-5, RING domain protein RCS-1, and F-box proteins FBXA-75, FBXA-158 to promote resistance to heat shock. This thermotolerance phenotype is dependent on neddylation of CUL-6 by NEDD8 conjugation. The model is adapted from Panek *et al.*, 2020, PNAS.

B) Fraction of survival for wild-type, *pals-22* mutant, *pals-22; cul-6* double mutant, and animals with *fbxa-158* deletion in a wild-type and a *pals-22* mutant background after heat shock treatment - following a 15-minute ramp up period from 25°C, animals were exposed to 2 hours of heat shock treatment at 37.5 °C (hereafter referred to as 2h heat shock treatment). Fraction of animals alive after heat shock was scored after 24 hours recovery at 20°C post heat shock treatment. ***$P < 0.001$, n.s. $P > 0.05$, one-way ANOVA with Tukey's post hoc multiple comparisons test.

C) Fraction of survival of wild-type, CUL-6 overexpressed animals, and animals with *fbxa-75* deletion in a wild-type and a CUL-6 overexpressed background. ***$P < 0.001$, **$P < 0.01$, n.s. $P > 0.05$, one-way ANOVA with Tukey's post hoc multiple comparisons test. (B) and (C) were reproduced from Panek *et al.*, 2020, PNAS.

Figure 1

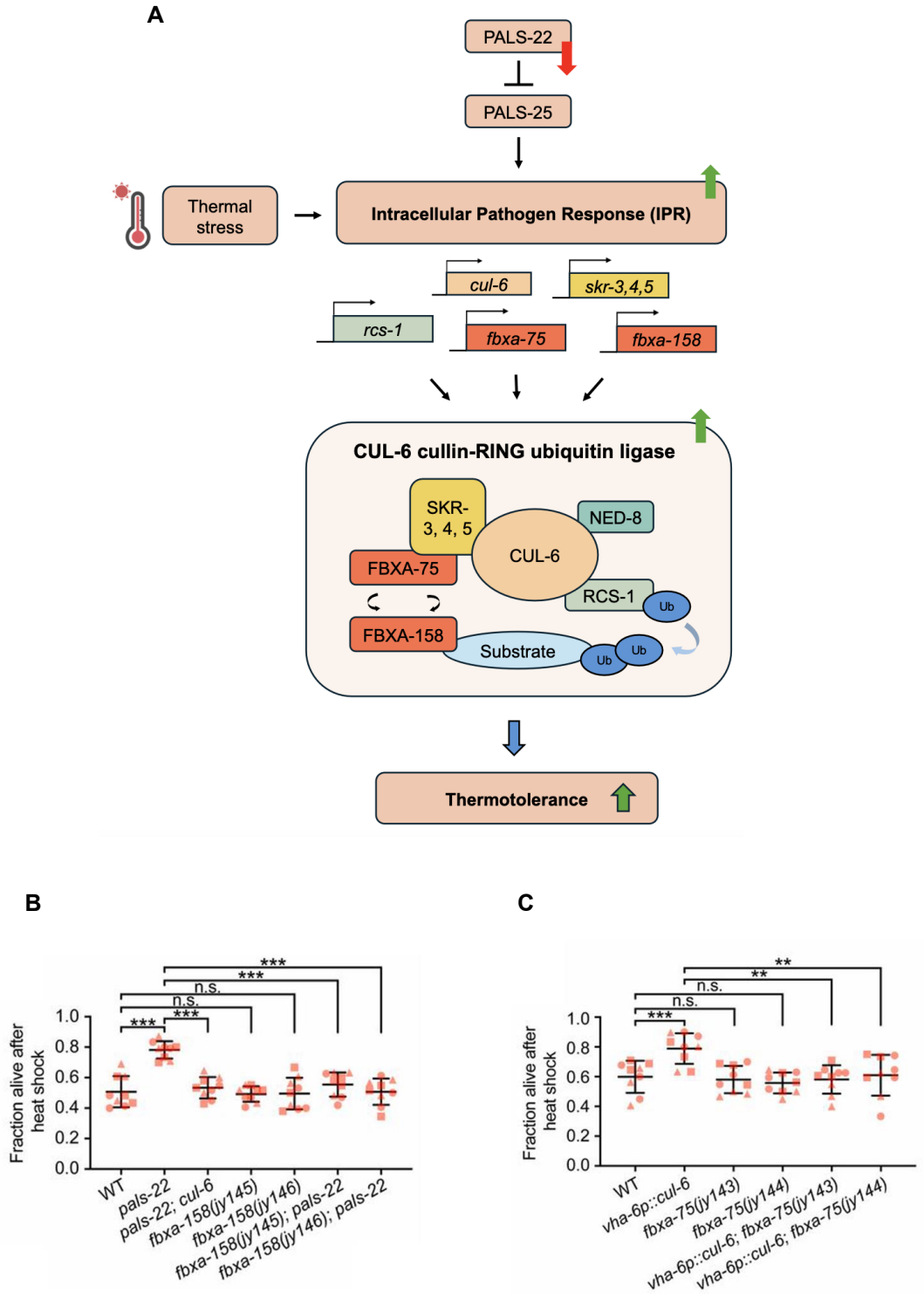
A
PALS-22
PALS-25
Thermal stress
Intracellular Pathogen Response (IPR)
cul-6
skr-3,4,5
rcs-1
fbxa-75
fbxa-158
CUL-6 cullin-RING ubiquitin ligase
SKR-3, 4, 5
NED-8
CUL-6
FBXA-75
RCS-1
Ub
FBXA-158
Substrate
Ub
Ub
Thermotolerance
B
Fraction alive after heat shock
1.0
0.8
0.6
0.4
0.2
0.0
***
***
n.s.
n.s.
***
WT
pals-22
pals-22; cul-6
fbxa-158(jy145)
fbxa-158(jy146)
fbxa-158(jy145); pals-22
fbxa-158(jy146); pals-22
C
Fraction alive after heat shock
1.0
0.8
0.6
0.4
0.2
0.0
**
**
n.s.
n.s.
***
WT
vha-6p::cul-6
fbxa-75(jy143)
fbxa-75(jy144)
vha-6p::cul-6; fbxa-75(jy143)
vha-6p::cul-6; fbxa-75(jy144)

Figure 2: HSP-90 is likely targeted for ubiquitylation by the CUL-6 ubiquitin ligase, leading to its degradation in the lysosome to promote thermotolerance.

A) Fraction of survival after a 1h 45 min heat shock treatment of wild-type animals and HSP-90::RFP$^{int\text{-}OE}$ animals in a wild-type, *cul-6* deletion, CUL-6$^{int\text{-}OE}$, and a neddylation-deficient CUL-6(K673R)$^{int\text{-}OE}$ background. **p < 0.01, ***p < 0.001, and ****p < 0.0001, A one-way ANOVA with Tukey's multiple comparisons test.
B) Quantification of RFP intensity of HSP-90::RFP$^{int\text{-}OE}$ animals in strain backgrounds listed in (A).
C) A model of CUL-6 mediated degradation of HSP-90 promoting thermotolerance when the IPR is active.
(A)– (C) were reproduced from Bardan Sarmiento *et al*., 2024., Cell Reports.

Figure 2

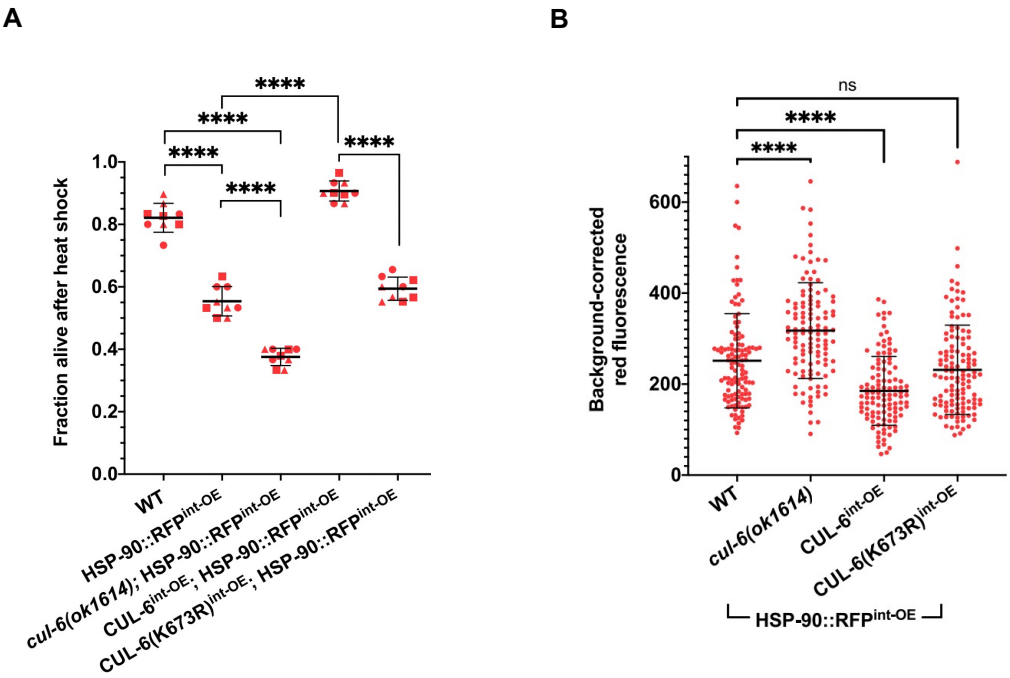
A
B
Fraction alive after heat shock
1.0
0.8
0.6
0.4
0.2
0.0
****
****
****
****
****
WT
HSP-90::RFPint-OE
cul-6(ok1614); HSP-90::RFPint-OE
CUL-6int-OE; HSP-90::RFPint-OE
CUL-6(K673R)int-OE; HSP-90::RFPint-OE
Background-corrected red fluorescence
600
400
200
0
ns
****
****
WT
cul-6(ok1614)
CUL-6int-OE
CUL-6(K673R)int-OE
HSP-90::RFPint-OE

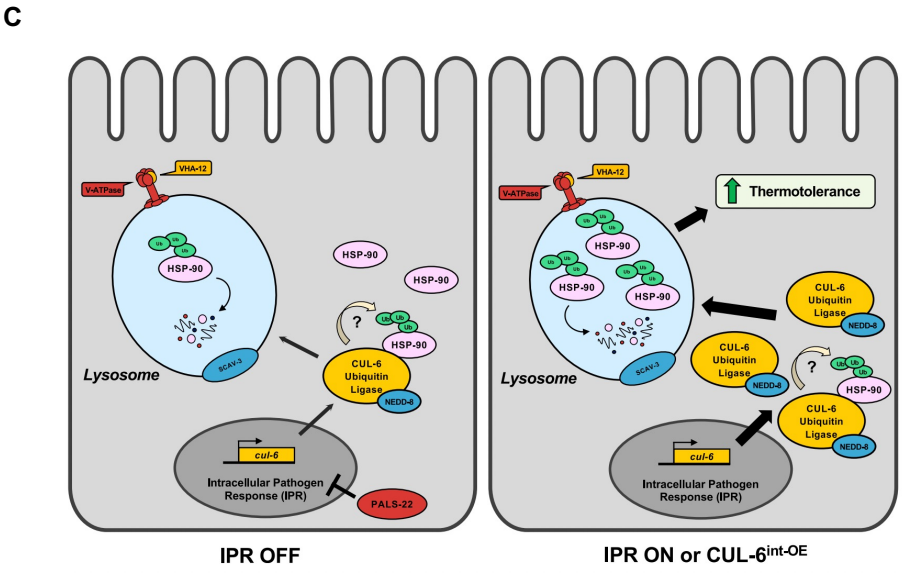
C
VHA-12
V-ATPase
HSP-90
Lysosome
SCAV-3
CUL-6 Ubiquitin Ligase
NEDD-8
cul-6
Intracellular Pathogen Response (IPR)
PALS-22
Thermotolerance
IPR OFF
IPR ON or CUL-6int-OE

Figure 3: The effects of *fbxa-75* and *fbxa-158* mutations on thermotolerance in a HSP-90::RFP^{int-OE} background.

A) Fraction of survival after 1h 45 min heat shock treatment of wild-type animals and HSP-90::RFP^{int-OE} animals with *cul-6*, *fbxa-75(jy143)*, and *fbxa-158(jy146)* deletion. Each dot represents a plate of approximately 30 animals, with 3 plates tested per day, across three independent experiments.

B) Quantification of HSP-90::RFP intensity of HSP-90::RFP^{int-OE} animals in different strain backgrounds: wild type, *cul-6(ok1614)* deletion, CUL-6^{int-OE}, *fbxa-75(jy143)* deletion, *fbxa-158(jy146)* deletion, *rcs-1(jy105)* deletion, *fbxa-158(jy146); fbxa-75(jy143)* double mutant, *fbxa-75(jy143); cul-6(ok1614)* double mutant. The experiment was performed in one replicate. P-values are determined by Kruskal Wallis test with Dunn's multiple comparisons test. ***$p < 0.001$, ****$p < 0.0001$.

C) Fraction of survival after 1h 45 min heat shock treatment of HSP-90::RFP^{int-OE} animals after RNAi treatment targeting *fbxa-11*, *fbxa-54*, *fbxa-188*. Each dot represents a plate of approximately 30 animals, with 3 plates tested per day, across three independent experiments. ****$p < 0.0001$, p-values are determined by one-way ANOVA with Tukey's multiple comparisons test.

(A)– (C) unpublished data, Mario Bardan Sarmiento.

Figure 3

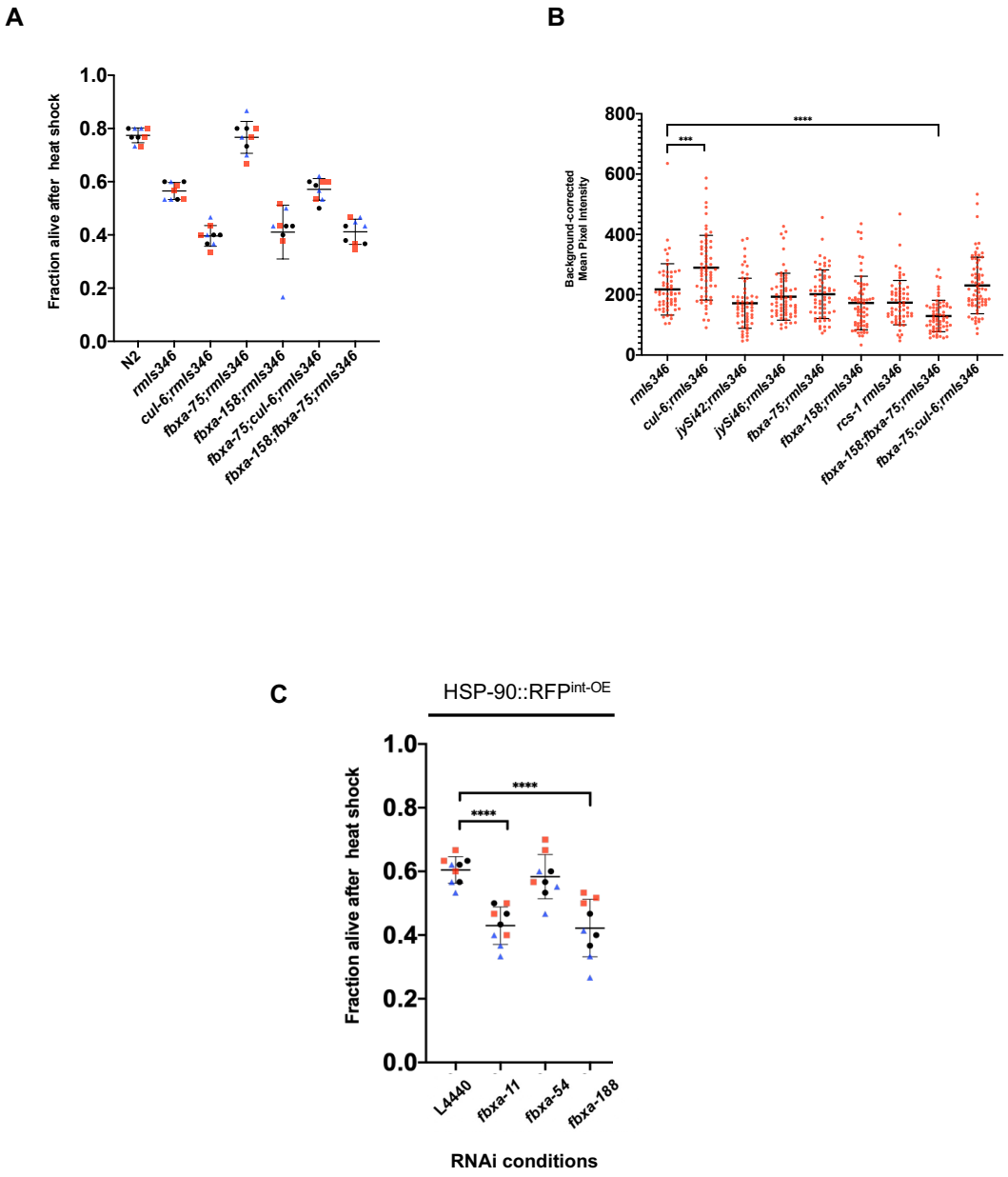
A
Fraction alive after heat shock
1.0
0.8
0.6
0.4
0.2
0.0
N2
rmIs346
cul-6;rmIs346
fbxa-75;rmIs346
fbxa-158;rmIs346
fbxa-75;cul-6;rmIs346
fbxa-158;fbxa-75;rmIs346
B
Background-corrected Mean Pixel Intensity
800
600
400
200
0
***
****
rmIs346
cul-6;rmIs346
jySi42;rmIs346
jySi46;rmIs346
fbxa-75;rmIs346
fbxa-158;rmIs346
rcs-1 rmIs346
fbxa-158;fbxa-75;rmIs346
fbxa-75;cul-6;rmIs346
C
HSP-90::RFPint-OE
Fraction alive after heat shock
1.0
0.8
0.6
0.4
0.2
0.0
****
****
L4440
fbxa-11
fbxa-54
fbxa-188
RNAi conditions

RESULTS

Figure 4: RNAi against *fbxa-11* increases HSP-90::RFP level and decreases survival post heat shock treatment specifically in the HSP-90::RFP^{int-OE} strain background.

A) Representative fluorescent images of HSP-90::RFP^{int-OE} animals after RNAi knockdown of the different F-box genes.
B) Fold change of quantified whole-animal RFP signal of HSP-90::RFP^{int-OE} animals after RNAi knockdown of the different F-box genes, normalized to L4440(OP50) vector control-treated animals in each replicate. n= 46-50 animals quantified. Experiments were performed in triplicate, each replicate performed on independent days. P-values are determined by Kruskal Wallis test with Dunn's multiple comparisons test. **$p < 0.01$, ****$p < 0.0001$.
C) Survival of wild-type animals after RNAi knockdown of the different F-box genes, normalized to L4440(OP50) vector control-treated animals in each replicate and subjected to 2h heat shock treatment. Each dot represents a plate of approximately 30 animals, with 3 plates tested per day, across three independent experiments.

Figure 4

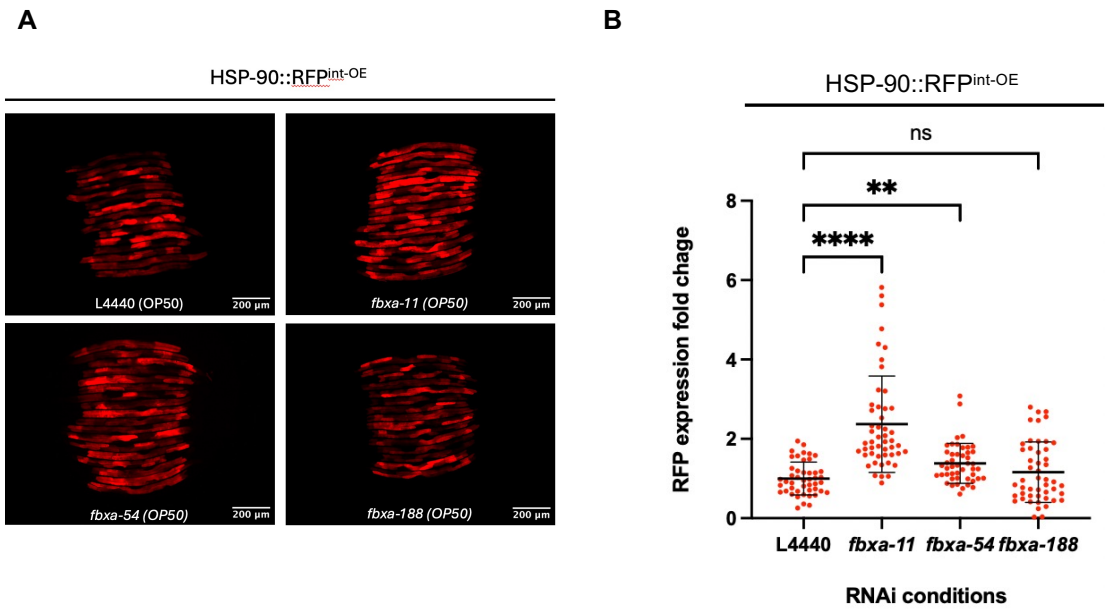
A
HSP-90::RFPint-OE
L4440 (OP50)
fbxa-11 (OP50)
fbxa-54 (OP50)
fbxa-188 (OP50)
200 µm
B
HSP-90::RFPint-OE
ns
**
****
RFP expression fold chage
0
2
4
6
8
L4440
fbxa-11
fbxa-54
fbxa-188
RNAi conditions

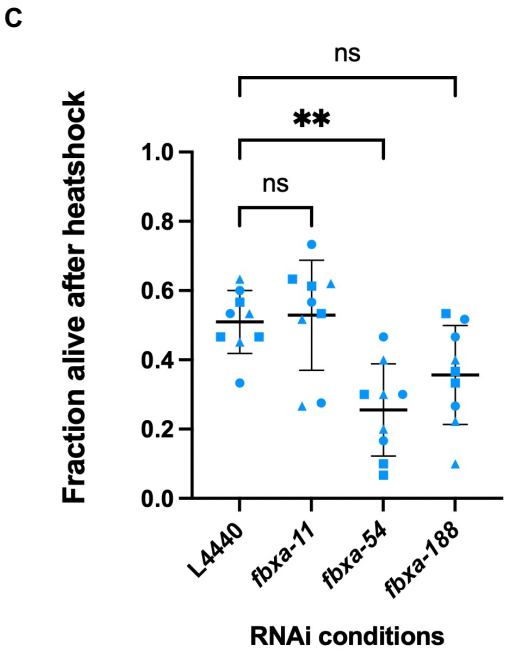
C
ns
**
ns
Fraction alive after heatshock
0.0
0.2
0.4
0.6
0.8
1.0
L4440
fbxa-11
fbxa-54
fbxa-188
RNAi conditions

Work from Mr. Bardan Sarmiento identified FBXA-11 as a candidate F-box protein acting in a CUL-6 ubiquitin ligase complex to target HSP-90 for degradation to promote thermotolerance. His preliminary imaging of HSP-90::RFP suggested that *fbxa-11* RNAi caused increased HSP-90::RFP^{int-OE} levels (not shown). To confirm this observation, I performed quantification of HSP-90::RFP^{int-OE} levels after RNAi knock-down of *fbxa-11*, as well as *fbxa-54* and *fbxa-188*. Here I found that *fbxa-11* RNAi treatment induces more than a 2-fold increase in HSP-90::RFP levels compared to L4440 control vector treated animals (Figure 4A, 4B). I found that *fbxa-54* RNAi caused a more modest increase in HSP-90::RFP levels, while *fbxa-188* RNAi had no significant effect on HSP-90::RFP levels. Altogether these results confirmed *fbxa-11* might act as a substrate-binding adapter protein for a CUL-6 ubiquitin ligase that targets HSP-90 for degradation, given that knock-down of *fbxa-11* caused an increase in HSP-90::RFP^{int-OE} levels.

Next, I further assessed the impacts of *fbxa-11* RNAi on thermotolerance. Given that loss of *cul-6* causes a decrease in thermotolerance in the presence of HSP-90::RFP^{int-OE} but not in wild-type strain background, I investigated whether the same phenotype was seen with loss of *fbxa-11*. Here I found that *fbxa-11* RNAi had no significant effect on thermotolerance in a wild-type background, although *fbxa-54* RNAi did decrease thermotolerance, which might be a subject for future study (Figure 4C). For the purposes of investigating *fbxa*-11, however, these findings were consistent with the model that FBXA-11 could act in a CUL-6 ubiquitin ligase complex to target HSP-90. In particular, similar to CUL-6, the loss of FBXA-11 decreased thermotolerance in the presence of HSP-90::RFP^{int-OE}, but not in its absence.

Figure 5: Characterization of the impact of *fbxa-11(tm13959)* on thermotolerance in the presence and absence of HSP-90 overexpression.

A) Gene structure and predicted amino acid sequence of *fbxa-11(tm13959)* mutant from knock-out consortium. Exons represented by blue boxes, start codon indicated by arrow.
B) Amino acid sequence alignment between predicted protein produced by wild-type *fbxa-11* and *fbxa-11(tm13959)* mutant. Alignment was performed using the EMBL-EBI Job Dispatcher sequence analysis tools framework (https://www.ebi.ac.uk/jdispatcher).
C) Fraction of survival of wild-type, *fbxa-11(tm13959)*, HSP-90::RFP^{int-OE}, and HSP-90::RFP^{int-OE} animals in a *fbxa-11(tm13959)* mutant background plated on NGM + OP50-1 plates and subjected to a 2h heat shock treatment. Experiments were performed in triplicate, each replicate performed on independent days.
D) Survival of wild-type, *fbxa-11(tm13959)*, HSP-90::RFP^{int-OE}, and HSP-90::RFP^{int-OE} animals in a *fbxa-11(tm13959)* mutant background plated on L4440(OP50) seeded RNAi plates and subjected to a 1h 45 min heat shock treatment. Experiments were performed in duplicate, each replicate performed on independent days.

For (C) – (D), each dot represents scoring from a culture plate with a set of 30 animals, different shapes represent different experimental replicates. Mean fraction alive of the triplicate is represented by black bar with error bars as SD. P-values are determined by one-way ANOVA with Tukey's multiple comparisons test. **$p < 0.01$, ***$p < 0.001$, and ****$p < 0.0001$.

Figure 5

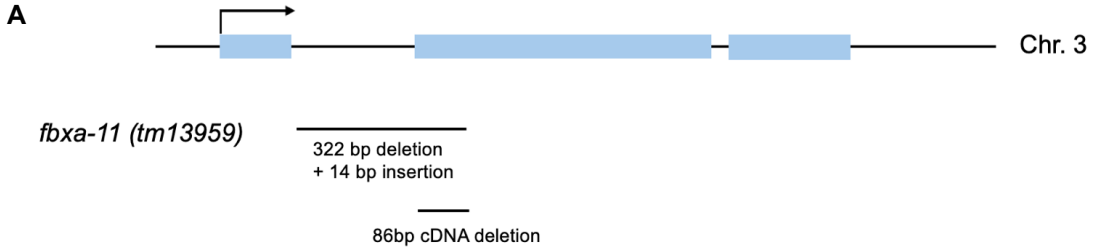

B

```
# Aligned_sequences: 2
# 1: EMBOSS_001
# 2: EMBOSS_001
# Matrix: EBLOSUM62
# Gap_penalty: 10.0
# Extend_penalty: 0.5
#
# Length: 296
# Identity:     268/296 (90.5%)
# Similarity:   269/296 (90.9%)
# Gaps:          24/296 ( 8.1%)
# Score: 1356.5
#
#
#=======================================

EMBOSS_001         1 MSTLLDMPVEIGKLVLKRMKPVERFVL------------------------     27
                     ||||||||||||||||||||||||||.|.
EMBOSS_001         1 MSTLLDMPVEIGKLVLKRMKPVERLVCRKVCRSLRTAVDSFGIRFNSVSV     50

EMBOSS_001        28 -MDDDYVLMDLNGLSIKYKSEENGTSAVYCNGKRIAREEDYLKVAFEDLM     76
                      :.||||||||||||||||||||||||||||||||||||||||||||||||
EMBOSS_001        51 DLYDDYVLMDLNGLSIKYKSEENGTSAVYCNGKRIAREEDYLKVAFEDLM    100

EMBOSS_001        77 AVMDQTSQLCFRNKRKELLNSITSVTDILKNKENLCVKEILLNTFSFDDA    126
                     ||||||||||||||||||||||||||||||||||||||||||||||||||||
EMBOSS_001       101 AVMDQTSQLCFRNKRKELLNSITSVTDILKNKENLCVKEILLNTFSFDDA    150

EMBOSS_001       127 LLILPCFNAQVLESIELWEAAPIDHCERLTGLDQWKNAKRFRTHDSRFQN    176
                     ||||||||||||||||||||||||||||||||||||||||||||||||||||
EMBOSS_001       151 LLILPCFNAQVLESIELWEAAPIDHCERLTGLDQWKNAKRFRTHDSRFQN    200

EMBOSS_001       177 EKLQIGQLFHFEKFQVEFDNFSILDVTKVKEDLLKRSEFKECSLIIGRFD    226
                     ||||||||||||||||||||||||||||||||||||||||||||||||||||
EMBOSS_001       201 EKLQIGQLFHFEKFQVEFDNFSILDVTKVKEDLLKRSEFKECSLIIGRFD    250

EMBOSS_001       227 STPFKIAQLFKPDVAEDMKYEIKYSVDNKIFVIFINRQVFCCELM*    272
                     ||||||||||||||||||||||||||||||||||||||||||||||
EMBOSS_001       251 STPFKIAQLFKPDVAEDMKYEIKYSVDNKIFVIFINRQVFCCELM*    296
```

Predicted *fbxa-11(tm13959)* amino acid sequence

Reference, wild-type *fbxa-11* amino acid sequence

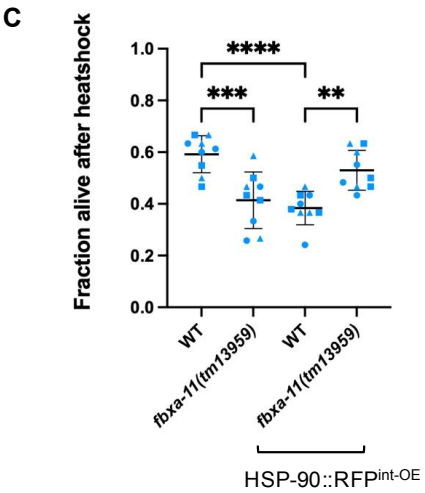

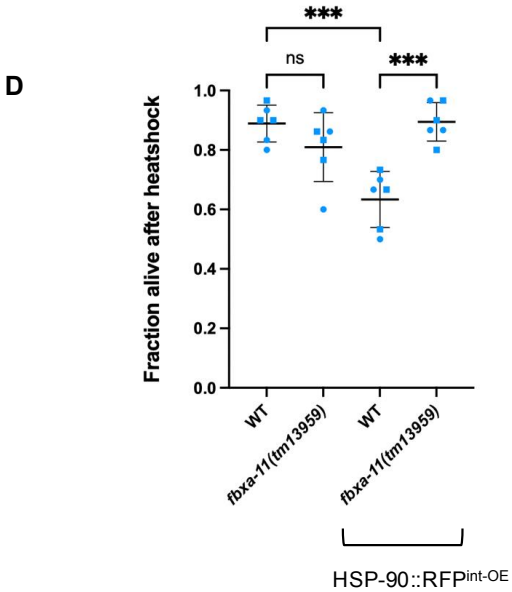

In order to complement the RNAi analysis and confirm that loss of *fbxa-11* causes decreased thermotolerance, I sought to analyze *fbxa-11* mutants. To this end, I obtained the *fbxa-11(tm13959)* mutant from the National BioResource Project of Japan (Yamazaki et al., 2010). This mutant has a 322 bp deletion and 14 bp insertion spanning the first intron and second exon of *fbxa-11* (Figure 5A). To determine the impact of this mutation on FBXA-11 amino acid sequence, I performed pairwise sequence alignment of the predicted FBXA-11 mutant protein with the wild-type FBXA-11 protein (Figure 5B). The wild-type FBXA-11 protein is predicted to have 296 amino acids, and the *fbxa-11(tm13959)* mutation is predicted to cause an in-frame deletion of 24 amino acids in the N-terminus (Figure 5B).

I backcrossed the *fbxa-11* mutant strain into the N2 wild-type background and into the HSP-90::RFP$^{int\text{-}OE}$ background. (Of note I genotyped for the *fbxa-11(tm13959)* allele and the HSP-90::RFP$^{int\text{-}OE}$ allele, but not the three other alleles found in the original *fbxa-11(tm13959)* strain, so their identity is unknown, see Table 1). I then tested the backcrossed *fbxa-11(tm13959)* mutant in both strain backgrounds with two heat shock paradigms, a longer heat shock (Figure 5C) and a shorter heat shock to accommodate the higher heat shock susceptibility of the HSP-90$^{int\text{-}OE}$ strains (Figure 5D). First, in contrast to *fbxa-11* RNAi, I found that *fbxa-11(tm13959)* in the wild-type background decreased thermotolerance compared to vector-treated control (Figure 5C). Next, also in contrast to *fbxa-11* RNAi, which caused decreased thermotolerance in a the HSP-90::RFP$^{int\text{-}OE}$ background, I found that *fbxa-11(tm13959)* caused increased thermotolerance in the HSP-90::RFP$^{int\text{-}OE}$ background (Figure 5D). Therefore, in general, the *fbxa-11(tm13959)* mutant had opposite effects from *fbxa-11* RNAi on thermotolerance.

Figure 6: Characterization of the impact of *fbxa-11(jy194)* and *fbxa-11* RNAi on thermotolerance in the presence and absence of HSP-90 overexpression.

A) The schematic representation of CRISPR/Cas9 mediated deletion strategy of *fbxa-11.* Locations of the two single guide RNA (sgRNA 1 and 2) relative to the coding region (exons are indicated by blue boxes) are indicated by orange arrows. The sgRNA binding regions are underlined with orange, and the PAM regions are underlined with blue.

B) Alignment of the sequences of wild type *fbxa-11* coding region and that of the *jy194* deletion mutant acquired by Sanger sequencing that demonstrates likely non-homologous end-joining (NHEJ) repair at cut sites. Nucleotides highlighted in dark red on the *jy194* mutant sequence tracing indicates mismatches compared to the reference, wild-type *fbxa-11* sequences. The bottom chromatogram represents selected portion of the *jy194* sequence tracing spanning the cut sites and the likely NHEJ repair region. The distance between the upstream cut site to the first exon is 86 bp, and the distance between the last exon and the likely NHEJ initiation site is 12 bp.

C) Fraction of survival of wild-type, *fbxa-11(jy194)*, HSP-90::RFP$^{int\text{-}OE}$, and HSP-90::RFP$^{int\text{-}OE}$ animals with the *fbxa-11(jy194)* knockout plated on L4440(OP50) seeded RNAi plates and subjected to a 1h 45 min heat shock treatment.

Experiment was performed in triplicate, each replicate performed on independent days. Each dot represents scoring from a culture plate with a set of 30 animals, different shapes represent different experimental replicates. Mean fraction alive of the triplicate is represented by black bar with error bars as SD. P-values are determined by one-way ANOVA with Tukey's multiple comparisons test. ****$p < 0.0001$.

D) Survival of HSP-90::RFP$^{int\text{-}OE}$ and HSP-90::RFP$^{int\text{-}OE}$ with the *fbxa-11(jy194)* deletion, after treatment with L4440(OP50) control and *fbxa-11(OP50)* RNAi and subjected to 1h 55 min heat shock treatment.

Experiment was performed in quintuplicate, each replicate performed on independent days. Each dot represents scoring from a culture plate with a set of 30 animals, different shapes represent different experimental replicates. Mean fraction alive of the triplicate is represented by black bar with error bars as SD. P-values are determined by one-way ANOVA with Tukey's multiple comparisons test. *$p < 0.05$, **$p < 0.01$.

Figure 6

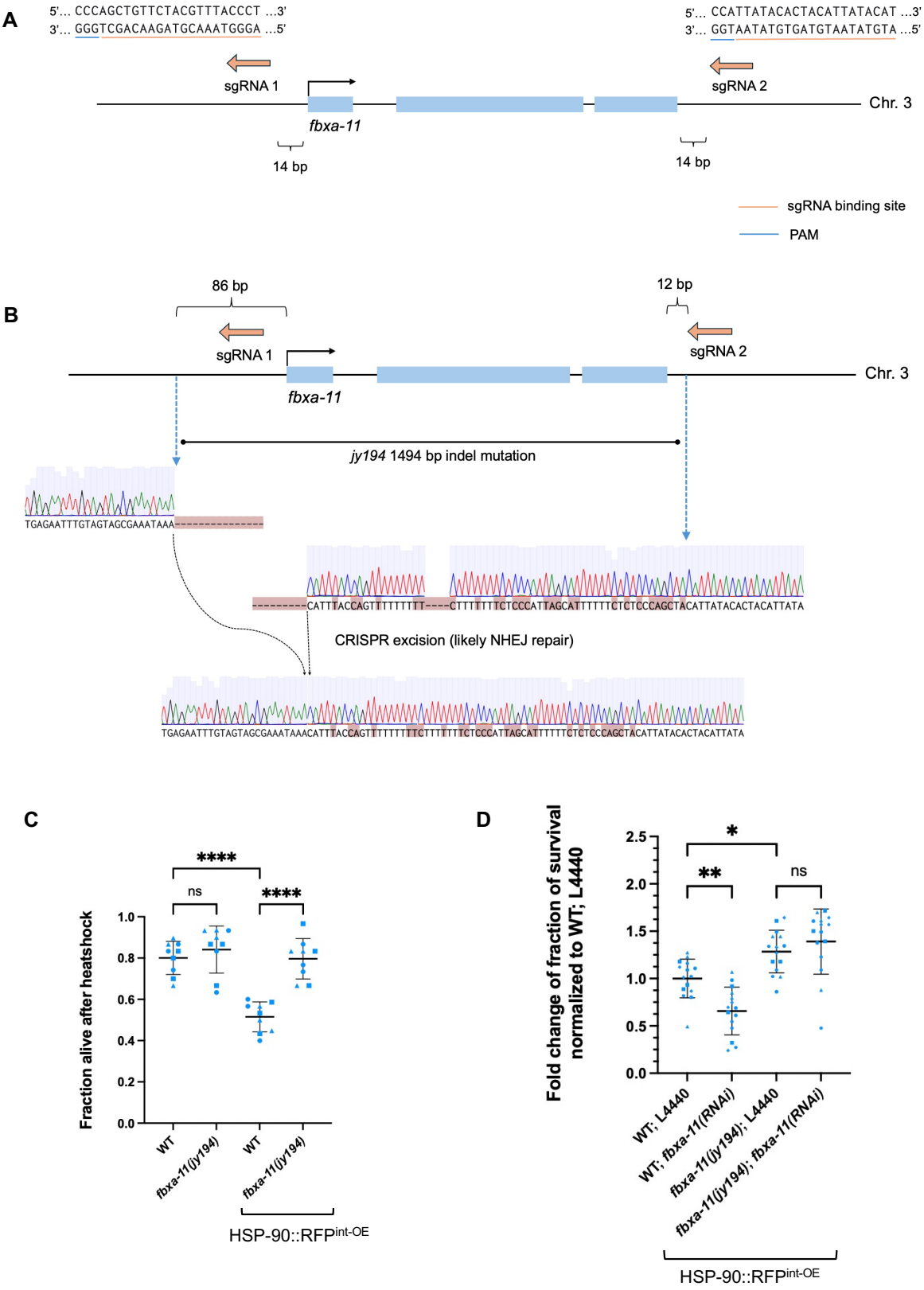
A
5'... CCCAGCTGTTCTACGTTTACCCT ...3'
3'... GGGTCGACAAGATGCAAATGGGA ...5'
5'... CCATTATACACTACATTATACAT ...3'
3'... GGTAATATGTGATGTAATATGTA ...5'
sgRNA 1
sgRNA 2
Chr. 3
fbxa-11
14 bp
14 bp
sgRNA binding site
PAM
B
86 bp
12 bp
sgRNA 1
sgRNA 2
Chr. 3
fbxa-11
jy194 1494 bp indel mutation
TGAGAATTTGTAGTAGCGAAATAAA----------
----------CATTTACCAGTTTTTTTTT----CTTTTTTTCTCCCATTAGCATTTTTTCTCTCCCAGCTACATTATACACTACATTATA
CRISPR excision (likely NHEJ repair)
TGAGAATTTGTAGTAGCGAAATAAACATTTACCAGTTTTTTTTCTTTTTTTCTCCCATTAGCATTTTTTCTCTCCCAGCTACATTATACACTACATTATA
C
Fraction alive after heatshock
****
ns
****
1.0
0.8
0.6
0.4
0.2
0.0
WT
fbxa-11(jy194)
WT
fbxa-11(jy194)
HSP-90::RFPint-OE
D
Fold change of fraction of survival normalized to WT; L4440
*
**
ns
2.5
2.0
1.5
1.0
0.5
0.0
WT; L4440
WT; fbxa-11(RNAi)
fbxa-11(jy194); L4440
fbxa-11(jy194); fbxa-11(RNAi)
HSP-90::RFPint-OE

Because *fbxa-11(tm13959)* should only cause a partial deletion in the FBXA-11 protein, and also because the *fbxa-11(tm13959)* strain had the possibility of other mutations in the background, I sought to generate a full deletion mutant through CRISPR-Cas9-mediated genome editing. I designed two sgRNA flanking the coding region of *fbxa-11,* injected them with Cas9 enzyme and genotyped progeny for the presence of an *fbxa-11* deletion (Figure 6A). Here I obtained allele *jy194*, which has a deletion of the *fbxa-11* coding region, together with 57 additional nucleotides likely included through the process of non-homologous end-joining repair at the CRISPR editing cut site. Given the DNA content at this locus, the *fbxa-11(jy194)* allele is likely a null allele and should produce no functional FXBA-11 protein (Figure 6B). Next, I backcrossed *fbxa-11(jy194)* into the N2 wild-type background and into the HSP-90::RFP$^{int\text{-}OE}$ background and tested thermotolerance with the shorter heat shock paradigm. Similar to results with the partial deletion *fbxa-11(tm13959)* with the reduced heat shock time, I found relatively modest effects of *fbxa-11(jy194)* on thermotolerance in the wild-type background. Also similar to results with *fbxa-11(tm13959)* in the HSP-90$^{int\text{-}OE}$ background, I found *fbxa-11(jy194)* caused increased thermotolerance (Figure 6C).

Because the *fbxa-11(jy194)* full deletion mutant has the opposite thermotolerance phenotype as *fbxa-11* RNAi in the HSP-90$^{int\text{-}OE}$ background, I investigated whether *fbxa-11* RNAi may be causing phenotypes through off-target interference in other genes. If that were true, then *fbxa-11* RNAi should still cause phenotypes in the absence of an intact *fbxa-11* gene. To test this hypothesis, I treated the *fbxa-11(jy194)* mutant with *fbxa-11* RNAi and measured thermotolerance in the HSP-90$^{int\text{-}OE}$ background. First, I found, consistent with my prior results, that *fbxa-11(jy194)* increased thermotolerance compared to wild-type animals in this

background. Next, consistent with Mr. Bardan Sarmiento's results, I found that *fbxa-11* RNAi in this background caused decreased thermotolerance. Thus, the controls worked in these experiments. Interestingly, I found that *fbxa-11* RNAi treatment on the *fbxa-11(jy194*) animals did not cause decreased thermotolerance (Figure 6D). Preliminarily, this result indicates that the effects of *fbxa-11* RNAi on thermotolerance are not likely due to off-target effects, because they depend on a wild-type copy of *fbxa-11*. Thus, despite the conflicting results of *fbxa-11* RNAi and *fbxa-11* mutant analysis, my results indicate that the effect of *fbxa-11* RNAi on thermotolerance could in fact be due to on-target effects, and decreased expression of FBXA-11 protein. One potential explanation for the discrepancy between the thermotolerance phenotypes of *fbxa-11* RNAi and *fbxa-11* mutants could be that there is some form of compensation that occurs in *fbxa-11* mutants, which results in a phenotype distinct from *fbxa-11* RNAi. Different types of compensatory mechanisms in *fbxa-11* mutants and ways to test this hypothesis are considered in the Discussion.

Figure 7: Characterization of the impact of *fbxa-11(tm13959)*, *fbxa-11(jy194)*, and *fbxa-11* RNAi on HSP-90::RFP levels.

A) Quantification of RFP signal in the anterior intestine of HSP-90::RFP$^{int\text{-}OE}$ animals, and HSP-90::RFP$^{int\text{-}OE}$ animals with the *fbxa-11(tm13959)* mutation and *fbxa-11(jy194)* CRISPR knockout.
Experiment was performed in triplicate, each replicate performed on independent days. Each dot represents the RFP intensity of an animal. n = 156-172 animals were quantified. Mean fraction alive of the triplicate is represented by black bar with error bars as SD. P-values were determined by Kruskal Wallis test with Dunn's multiple comparisons test. ****$p < 0.0001$.

B) Representative fluorescent images of HSP-90::RFP$^{int\text{-}OE}$ and HSP-90::RFP$^{int\text{-}OE}$ with the *fbxa-11(jy194)* deletion treated with L4440 (OP50) empty vector control or *fbxa-11(OP50)* RNAi.

C) Fold change of quantified whole animal RFP signal of strains with their respective RNAi treatment shown in (B), normalized to L4440(OP50) treated HSP-90::RFP$^{int\text{-}OE}$ animals in each replicate. n= 58-66 animals quantified.
Experiments were performed in triplicate, each replicate performed on independent days. P-values are determined by Kruskal Wallis test with Dunn's multiple comparisons test. ***$p < 0.001$ and ****$p < 0.0001$.

Figure 7

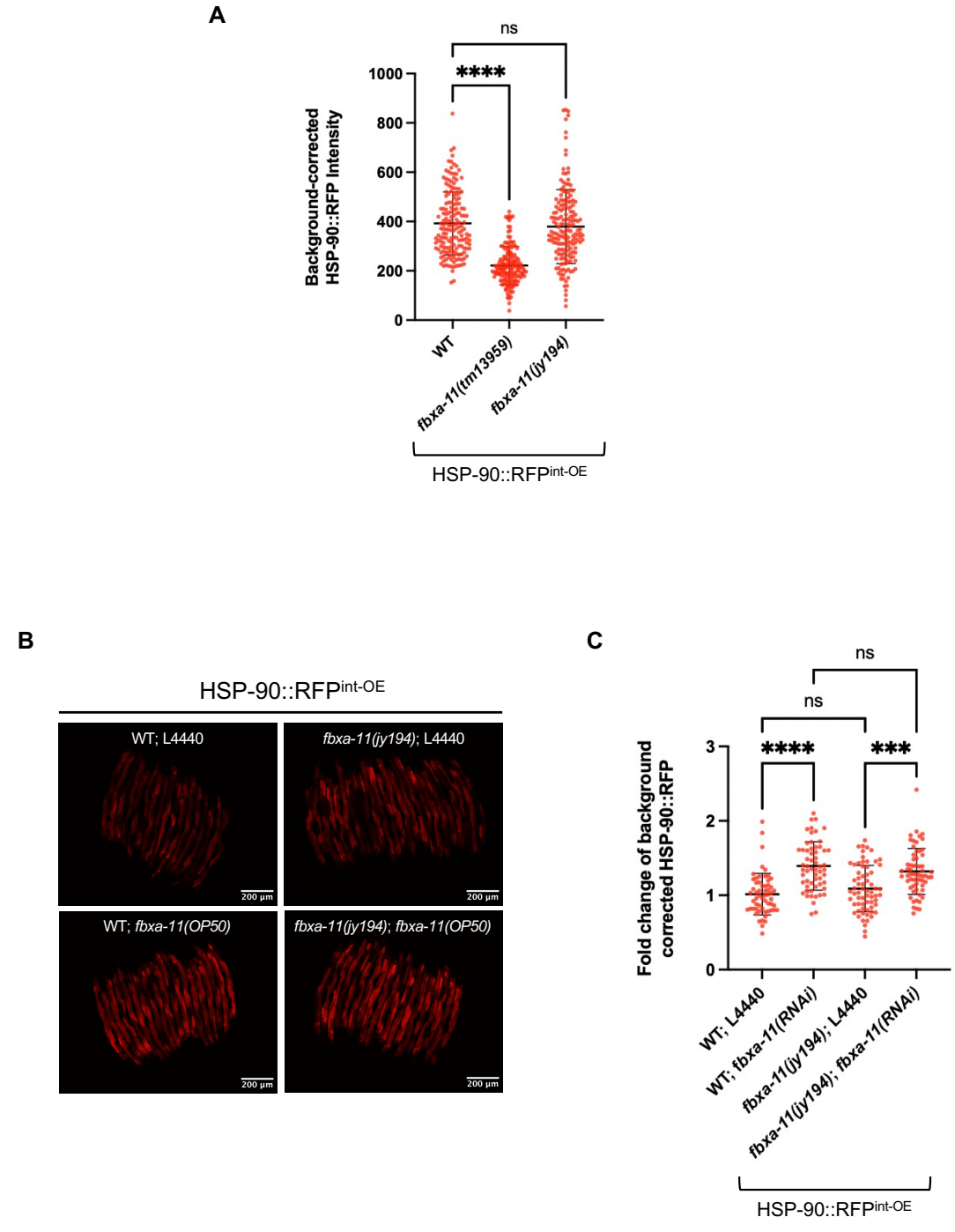
A
ns
****
Background-corrected HSP-90::RFP Intensity
1000
800
600
400
200
0
WT
fbxa-11(tm13959)
fbxa-11(jy194)
HSP-90::RFPint-OE
B
HSP-90::RFPint-OE
WT; L4440
fbxa-11(jy194); L4440
WT; fbxa-11(OP50)
fbxa-11(jy194); fbxa-11(OP50)
200 µm
C
ns
ns
****
***
Fold change of background corrected HSP-90::RFP
3
2
1
0
WT; L4440
WT; fbxa-11(RNAi)
fbxa-11(jy194); L4440
fbxa-11(jy194); fbxa-11(RNAi)
HSP-90::RFPint-OE

In addition to assessing thermotolerance, I also examined the impact of *fbxa-11(tm13959)* and *fbxa-11(jy194)* mutations on HSP-90::RFP^{int-OE} protein levels. If *fbxa-11* did encode a substrate-binding protein that is directly involved in the degradation of HSP-90, loss of *fbxa-11* should lead to an increase in HSP-90::RFP^{int-OE} levels. However, in contrast to the effects of *fbxa-11* RNAi and this model, I found that *fbxa-11(tm13959)* had lower HSP-90::RFP levels than wild-type animals, and the *fbxa-11(jy194)* had similar HSP-90::RFP levels as wild-type animals (Figure 7A). Because the full deletion mutant did not show an increase in HSP-90::RFP, there is a possibility that *fbxa-11* RNAi treatment had off-target effect that altered this phenotype. Indeed, treating the *fbxa-11(jy194)* mutant with *fbxa-11* RNAi in an HSP-90^{int-OE} background did increase HSP-90::RFP levels (Figure 7B, C). Thus, the impact of *fbxa-11* RNAi on HSP-90 levels appears to be due to off-target effects, in contrast to the impact of *fbxa-11* RNAi on thermotolerance, which did not seem to be due to off-target effects. Of note, there are likely many other CUL-6 ubiquitin ligase substrates in addition to HSP-90 that impact thermotolerance; see Discussion for more details.

Figure 8: Characterization of the impact of *fbxa-11(jy194)* on thermotolerance in a CUL-6 overexpression background.

Fraction of survival of wild-type, *fbxa-11(jy194)*, CUL-$6^{int\text{-}OE}$, and CUL-$6^{int\text{-}OE}$ animals with the *fbxa-11(jy194)* knockout plated on L4440(OP50) seeded RNAi plates and subjected to a 2h heat shock treatment.

Experiment was performed in triplicate, each replicate performed on independent days. Each dot represents scoring from a culture plate with a set of 30 animals, different shapes represent different experimental replicates. Mean fraction alive of the triplicate is represented by black bar with error bars as SD. P-values are determined by one-way ANOVA with Tukey's multiple comparisons test. *$p < 0.05$, ****$p < 0.0001$.

Figure 8

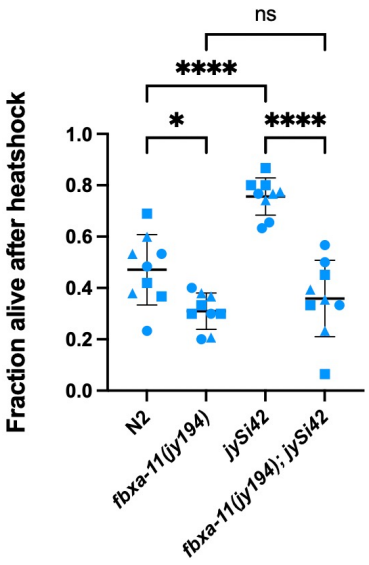
ns
****
*
****
Fraction alive after heatshock
1.0
0.8
0.6
0.4
0.2
0.0
N2
fbxa-11(jy194)
jySi42
fbxa-11(jy194); jySi42

Finally, I investigated the impact of my newly generated *fbxa-11(jy194)* deletion mutation on thermotolerance in an "IPR ON" background, which is the original context in which the CUL-6 ubiquitin ligase complex was defined. Previously it was found that *fbxa-11* RNAi did not alter the thermotolerance phenotype in a *pals-22* mutant background, where CUL-6 is overexpressed (Panek et al., 2020). However, as *fbxa-11* RNAi appeared to have off-target effects, and RNAi can sometimes have low efficacy, I decided to assess whether crossing *fbxa-11(jy194)* into a CUL-6 overexpression background might reveal a role for FBXA-11 in this context. The intestinal overexpression of CUL-6 alone in the CUL-6$^{int\text{-}OE}$ strain was previously shown to increase thermotolerance (Panek et al., 2020). If *fbxa-11* deletion ablated that increased thermotolerance, then it could be supporting evidence that *fbxa-11* potentially acts in the CUL-6-driven pathway. After 2 hours of heat shock treatment, I observed that *fbxa-11(jy194)* deletion decreased the thermotolerance of CUL-6$^{int\text{-}OE}$ animals, suggesting that FBXA-11 promotes thermotolerance in this context (Figure 8). However, I also found that with the 2-hour heat shock treatment, *fbxa-11(jy194)* deletion also induces a modest decrease in thermotolerance in the wild-type background (Figure 8), which was not observed with the 1 hour 45-minute heat shock treatment (Figure 6C). The overall high survival post 1 hour 45-minute heat shock could have obscured the intermediately lower thermotolerance of *fbxa-11(jy194)* mutant in the wild-type background specifically. Altogether these data in both the wild-type and CUL-6 overexpression model indicate that in these contexts FBXA-11 acts to promote thermotolerance, similar to CUL-6.

DISCUSSION

F-box proteins are greatly expanded in the *C. elegans* genome compared to yeast, humans and several other organisms. These proteins work as part of SCF E3 ubiquitin ligase enzymes as interchangeable adapter proteins, which provide specificity to these ligases through their binding to and targeting of different substrates for ubiquitylation. The effects of ubiquitylation can vary depending on the context, but a common fate for ubiquitylated substrates is degradation. Thus, it is possible that *C. elegans* is able to target a large number of substrates for degradation with their large F-box protein repertoire. This feature likely offers *C. elegans* various survival advantages through fine-tuning regulation of substrate ubiquitylation thereby better protecting organismal proteostasis. It is also possible that co-evolving pathogens of *C. elegans* may have driven some of this expansion in the *C. elegans* genome, and some of these F-box proteins can target pathogen proteins for degradation. Although there may be over 520 F-box genes present in the *C. elegans* genome, the functions of many of them are currently unknown.

My results provided new insights into the role of a previously uncharacterized F-box protein, FBXA-11, on regulating thermotolerance, and demonstrated that its role could be dependent on different strain backgrounds. Prior work performed by Mr. Bardan Sarmiento identified that *fbxa-11* RNAi decreases thermotolerance in an HSP-90::RFP$^{int\text{-}OE}$ background and further increases the level of HSP-90::RFP (Figure 3C, 4A), suggesting that it may act as an adaptor protein in a CUL-6 ubiquitin ligase to target HSP-90 for ubiquitylation and subsequent degradation, to promote thermotolerance. To further investigate the role of FBXA-11 in thermotolerance, I tested *fbxa-11* RNAi in the wild-type background and found that it had no significant impact on thermotolerance, similar to what was reported in the *pals-22* background

(Figure 4C), and potentially suggests that FBXA-11 may act in an HSP-90-dependent manner to promote thermotolerance.

To build on the *fbxa-11* RNAi analysis, I used an existing partial deletion mutant *fbxa-11(tm13959)* and generated a null allele mutant for *fbxa-11(jy194)* via CRISPR-Cas9-mediated genome editing. In contrast to *fbxa-11* RNAi, both mutants showed decreased thermotolerance in the wild-type background (Figure 5C & 8) and increased thermotolerance in a HSP-90::RFP$^{int\text{-}OE}$ background (Figure 5D & 6C). More importantly, treating the *fbxa-11(jy194)* mutant with *fbxa-11* RNAi in the HSP-90$^{int\text{-}OE}$ background did not seem to further decrease the thermotolerance phenotype, suggested that the decreased thermotolerance observed in the HSP-90::RFP$^{int\text{-}OE}$ background following *fbxa-11* RNAi treatment may not be a result of RNAi off-target effect and was rather due to on-target knockdown of *fbxa-11* expression (Figure 6D). I further expanded the assessment of FBXA-11 to test its role in the CUL-6$^{int\text{-}OE}$ background to probe its relevance in an IPR-active background using the *fbxa-11(jy194)* null allele strain. Here I found that *fbxa-11* deletion suppresses the increase thermotolerance caused by CUL-6 overexpression, consistent with a role in promoting thermotolerance (Figure 8).

Of note, prior analysis with either mutant or RNAi analysis of *cul-6* yielded similar impacts on thermotolerance and HSP-90::RFP levels, but in the case of *fbxa-11* I found that these two approaches yielded differing results. Because of the discrepancy between the results with *fbxa-11* RNAi and mutant analysis, it would be worthwhile to explore the function of FBXA-11 with other techniques. For example, another approach to knockdown FBXA-11 would be through auxin-mediated degradation of FBXA-11 protein after tagging it with an auxin-inducible

degron (AID) (Martinez & Matus, 2020). This protein knockdown method allows for rapid and direct depletion of FBXA-11 proteins. In contrast, RNAi efficacy in protein knockdown may be impacted by the natural turnover rate of the protein of interest (Mocellin & Provenzano, 2004). The auxin-mediated degradation approach thus can lead to potentially better penetrance in phenotype compared to RNAi and also with minimal, unpredictable interference of potential off-target effects as observed with *fbxa-11* RNAi (Zhang et al., 2015). Querying the Sanger sequencing-confirmed nucleotide sequence of the *fbxa-11* RNAi clone on NCBI Nucleotide BLAST (BLASTN) returns multiple high confidence hits with other F-box genes: *fbxa-10* (E-value = 4e-13), *fbxa-55* (E-value = 3e-07), *fbxa-60* (E-value = 1e-05), *fbxa-59* (E-value = 2e-04), *fbxa-13* (E-value = 0.002), *fbxa-62* (E-value = 0.008), *fbxa-42* (E-value = 0.008). The precent identities of sequence regions of high homology ranges from 68.55% to 77.78%, covering a range of 62 to 160 nucleotide bases. A study suggested that at least 52% of F-box genes arose through tandem duplication, which contributes to the divergence in F-box genes in the *C. elegans* genome (Wang et al., 2021). Tandemly duplicated genes may be retained for selective advantages such as novel functions or beneficial redundancy (Bonthala & Stich, 2022). However, this could also imply that targeting F-box genes with RNAi could lead to unpredicted off-target effect due to the high sequence homology among F-box genes, as past studies had suggested that even partial complementary sequences within the siRNA seed region from nucleotide 2-8 may be sufficient to silence non-targeted genes (Kobayashi et al., 2022). This observation again highlights the importance of complementing RNAi studies with mutant analysis when exploring gene functions.

One potential hypothesis for lack of effect of *fbxa-11* RNAi in wild-type and *pals-22* mutants is that RNAi may have had low efficacy in these backgrounds, and somehow the residual protein was sufficient to prevent changes in thermotolerance. To investigate the efficacy of RNAi on FBXA-11 depletion, reduction of FBXA-11 protein following RNAi could be quantified via western blot analysis, although this technique would require generating antibodies against FBXA-11, or generating an epitope-tagged strain. On the other hand, the efficacy of *fbxa-11* RNAi impacting thermotolerance in an HSP-90::RFP$^{int\text{-}OE}$ background might be due to different expression levels of *fbxa-11* in this context. The expression level of *fbxa-11* mRNA in different strain backgrounds, and knockdown efficiency could be investigated using RT-qPCR (Onchuru & Kaltenpoth, 2019). *fbxa-11* is already known to be upregulated in *pals-22* mutants (Reddy et al., 2019), but its expression level in HSP-90::RFP$^{int\text{-}OE}$ is not known.

My findings so far point to the possibility that deletion of the *fbxa-11* gene in HSP-90::RFP$^{int\text{-}OE}$ background might be triggering a compensatory pathway, leading to an increase in thermotolerance not observed in wild-type and CUL-6$^{int\text{-}OE}$ background. One hypothesis to explain this difference between the mutant and RNAi-induced phenotype in specifically the HSP-90::RFP$^{int\text{-}OE}$ background could be genetic robustness (El-Brolosy & Stainier, 2017). For example, loss of *fbxa-11* may lead to increased expression of other F-box proteins that may be targeting an overlapping subset of substrates, or even a more diverse groups of substrates, leading to the increase in thermotolerance observed. Several studies have provided evidence for genetic compensation possibly responsible for differences in phenotypes between loss of function mutant and RNAi phenotypes. For instance, in mouse embryonic stem cells (mESCs), knockdown of *Importinα5* through short hairpin RNA (shRNA) reduces neural inhibition,

whereas mice with mutation in *Importinα5* show wild-type brain development, potentially due to the compensatory upregulation of another subtype, IMPORTINα4, that rescues the function (Shmidt et al., 2007). Other possibilities that could contribute to this discrepancy between RNAi and mutant phenotype in the HSP-90::RFP$^{int\text{-}OE}$ background may be recombination among F-box genes or alternative splicing among other F-box mRNA following the deletion. RNA-seq would be useful to provide more insights on potential gene expression changes or compensatory upregulation following *fbxa-11* deletion. After identifying potential genes of interests that are upregulated in the *fbxa-11* deletion mutant context, their transcriptional expression could be further confirmed via RT-qPCR before advancing to assess their roles with genetic assays.

Previous studies had found evidence that ubiquitin ligase components had different effects on thermotolerance in different strain backgrounds, which may be related to the different effects *fbxa-11* has in the different strain backgrounds. For instance, loss of CUL-6 only decreases thermotolerance in a *pals-22* loss of function mutant background and does not impact survival in a wild-type background (Reddy et al., 2017). Subsequently, loss of CUL-6 was found to also decrease thermotolerance in an HSP-90::RFP$^{int\text{-}OE}$ background (Figure 2A). Collectively, these findings point to how CUL-6 might act in an IPR-specific pathway and might interact with specifically HSP-90 to mediate thermotolerance, hence its loss leads to the different phenotypes observed in the different strain backgrounds.

Similar to CUL-6, past studies found that some F-box proteins' roles in regulating thermotolerance is also dependent on the respective strain backgrounds. In addition to FBXA-11, FBXA-75 and FBXA-158 had been examined due to their role as significant interactors with

CUL-6 (Panek et al., 2020). So far, the roles observed for the *fbxa-11* and the *fbxa-75* null allele share some similarities. In particular, they both lead to increased thermotolerance in the HSP-90::RFP^{int-OE} background (Figure 3A & 6C) and decreased survival in the CUL-6^{int-OE} background (Figure 1C & 8). Since the *fbxa-11* null allele could potentially be triggering a compensation pathway upregulating other F-boxes, future studies can explore whether knockdown methods such as *fbxa-75* RNAi or auxin-mediated degradation would induce a similar or different phenotype than observed with the *fbxa-75* null allele. If *fbxa-75* knockdown leads to decreased thermotolerance, opposite to what was observed with the mutant phenotype, there is a possibility that the removal of *fbxa-75* also could be triggering a compensatory mechanism specifically in the HSP-90::RFP^{int-OE} background and leads to the increased in thermotolerance we observed. If this is the case, future studies can also compare whether the compensatory gene upregulations caused by *fbxa-11* and *fbxa-75* cover a set of overlapping genes that is potentially working specifically in this HSP-90 specific background to promote thermotolerance.

Notably, Mr. Bardan Sarmiento also found that neither *fbxa-75* nor *fbxa-158* deletion significantly impacted the level of overexpressed HSP-90::RFP in the animals. While *fbxa-11* RNAi leads to increases in HSP-90::RFP in the HSP-90::RFP^{int-OE} background, analysis of *fbxa-11(jy194)* null allele mutant in this background demonstrates that *fbxa-11* deletion does not lead to an increase in HSP-90::RFP (Figure 7A). This result was further corroborated by the increase in HSP-90::RFP levels when treating the *fbxa-11(jy194)* mutant with *fbxa-11* RNAi (Figure 7B & C), suggesting that the increase in HSP-90::RFP induced by *fbxa-11* RNAi could be due to an off-target effect of the RNAi clone. Since the off-target effect does not further decrease survival

in the full deletion mutant, this suggests that the thermotolerance phenotype induced by *fbxa-11* RNAi is independent of potential interactions of *fbxa-11* targeting HSP-90 as a substrate. This points to the possibility that FBXA-11 could be interacting with other substrates of the CUL-6 complex to mediate thermotolerance. There are likely many different substrates in addition to HSP-90 that are targeted by the CUL-6 ubiquitin ligase, as E3 ubiquitin ligases could target a variety of different substrates under different cellular contexts, and a singular substrate could also be targeted by different ubiquitin ligases for ubiquitylation (Iconomou & Saunders, 2016). Therefore, future studies can explore what potential substrates might be targeted by FBXA-11 for degradation to improve thermotolerance. Identifying F-box substrates would be challenging due to the weak protein-protein interactions when they bind their substrates as well as the rapid subsequent degradation after the substrates are ubiquitylated (Jin et al., 2005; Yoshida et al., 2015). Future studies could consider biochemical approaches that are more sensitive for the detection of weak and transient substrate-adapter protein interactions, and potentially using multiple approaches to identify and validate the interaction between F-box proteins and the substrates of interest. One potential method that could alleviate the impact of rapid proteasomal degradation of ubiquitylated substrates is tandem ubiquitin-binding entity (TUBE) technology, which was proven useful in more reliable detection of F-box substrates by stabilizing ubiquitylation on the substrates and hindering their degradation, allowing for more reliable detection of adapter protein-substrate interactions (Yoshida et al., 2015).

Overall, my results present evidence for the potential role of FBXA-11 in improving thermotolerance by working as part of the CUL-6 ubiquitin ligase complex and potentially targeting HSP-90, as well as non-HSP-90 substrates. Future studies could explore mechanism of

action for FBXA-11 by identifying the substrates and also the SKR proteins with which it interacts. Through such studies, we could gain more insights on the complex proteostasis pathway *C. elegans* has developed to battle proteotoxic stress. Given the new understanding of FBXA-11 having a role in stress-response pathway and promoting proteostasis, if a new set of targeted substrates of FBXA-11 could be identified, it could provide exciting new directions in looking at how to strategically target those substrates in an aging or microbial infection context to improve host proteome integrity.

Figure 9: Model of the role of FBXA-11 mediating thermotolerance in the IPR pathway. FBXA-11 might work as part of the CUL-6 SCF E3 ligase to target substrate other than HSP-90 for ubiquitin-mediated degradation, increasing thermotolerance.

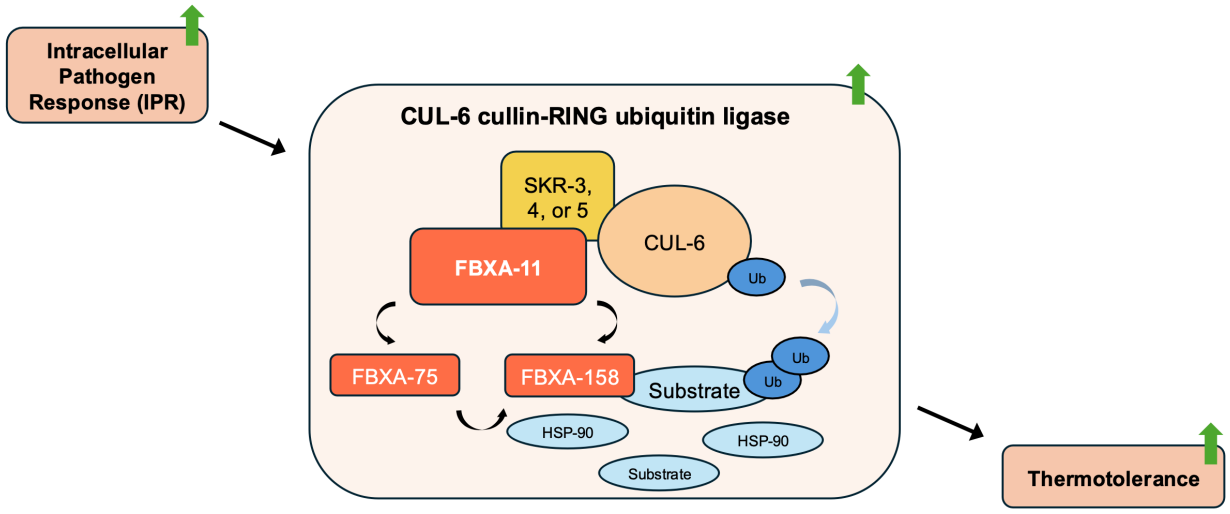

MATERIALS AND METHODS

Table 1: List of strains used in this thesis

Identifier	Genotype	Source
N2	Wild-type	Caenorhabditis Genetics Center
ERT1225	*rmIs317[hsp-90p::GFP]*	van Oosten-Hawle et al., 2013; backcrossed to N2 four times
ERT1247	*cul-6(ok1614) IV; rmIs317[hsp-90p::GFP]*	Generated by crossing ERT1225 *rmIs317[hsp-90p::GFP]* with ERT540 *cul-6(ok1614) IV*
ERT1248	*jySi42[pET499 (vha-6p::GFP::cul-6::unc-54 3' UTR, unc-119 (+)] II; unc-119(ed3) III; rmIs317[hsp-90p::GFP]*	Generated by crossing ERT1225 *rmIs317[hsp-90p::GFP]* with ERT571 *jySi42[pET499(vha-6p::GFP::cul-6::unc-54 3' UTR, unc-119(+))] II; unc-119(ed3) III*
ERT1249	*jySi46[pET688 (vha-6p::GFP::cul-6(K673R)::unc-54 3' UTR, unc-119 (+)] II; unc-119(ed3) III; rmIs317[hsp-90p::GFP]*	Generated by crossing ERT1225 *rmIs317[hsp-90p::GFP]* with ERT740 *jySi46[pET688(vha-6p::GFP::cul-6(K673R)::unc-54 3' UTR, unc-119(+))] II; unc-119(ed3) III*
ERT1236	*rmIs346[vha-6p::HSP-90::RFP]* - in the text, often referred to as HSP-90::RFP^{int-OE}	van Oosten-Hawle et al., 2013; backcrossed to N2 three times
FX23959	*FX23959[atm-1(tm5027) I; fbxa-11(tm13959) III; xpc-1(tm3886) IV; scrab-1(tm13960) V]*	National BioResource Project
ERT1294	*FX23959[atm-1(tm5027)? I; fbxa-11(tm13959) III; xpc-1(tm3886)? IV; scrab-1(tm13960)? V]; rmIs346[vha-6p::HSP-90::RFP]*	Backcross of FX23959 to N2 three times, genotyping for *tm13959* only
ERT1308	*fbxa-11(jy194) III*	Backcross of *fbxa-11(jy194)* animals newly generated by CRISPR-Cas9-mediated genome editing to N2 for three times
ERT1309	*fbxa-11(jy194) III; rmIs346[vha-6p::HSP-90::RFP]*	Generated by crossing ERT1308 *fbxa-11(jy194) III* into ERT1236 *rmIs346[vha-6p::HSP-90::RFP]*
ERT1337	*jySi42 [pET499 (vha-6p::GFP::cul-6::unc-54 3' UTR, unc-119 (+)] II; fbxa-11(jy194) III*	Generated by crossing ERT1308 *fbxa-11(jy194) III* into ERT571 *jySi42[pET499(vha-6p::GFP::cul-6::unc-54 3' UTR, unc-119(+))] II; unc-119(ed3) III*

Table 2: List of primers used in this thesis

Primer Name	Sequence	Melting Temperature (°C)	GC Content	Length (bp)
fbxa-11(tm13959) genotyping external forward	GTCGTCAAATCATGCGCCTG	65	55	20
fbxa-11(tm13959) genotyping external reverse	TTTTCCACTGGTCCAAGCCG	66	55	20
fbxa-11(tm13959) genotyping internal reverse	CCGTGAGGCTTCCTAAACTTCT	65	50	22
vha-6p::GFP::cul-6 MoSCI insertion forward	ACACCGACAAAGAATCTCCACCTG	67	50	24
vha-6p::GFP::cul-6 MoSCI insertion reverse	CGTATGTTGCATCACCTTCACCC	67	52	23
fbxa-11(jy194) genotyping external forward	GTCGTCAAATCATGCGCCTG	65	55	20
fbxa-11(jy194) genotyping external reverse	AACTCACAGGTCCTCGGGAT	65	55	20
fbxa-11(jy194) genotyping internal reverse	GCACAATTGTGAGGTTTGGTCC	65	50	22

***C. elegans* maintenance**

C. elegans nematodes were maintained and grown at 20°C on Nematode Growth Media (NGM) agar plates seeded with streptomycin-resistant *Escherichia coli* OP50-1.

Synchronization of *C. elegans*

To obtain synchronized *C. elegans* for fluorescent microscopy imaging (Figure 7A & Appendix A), gravid adult animals are collected in M9 buffer into a 15 mL conical tube. The tube was then centrifuged and the supernatant was removed until ~2 mL solution was left. 800 mL of 5.65–6% sodium hypochlorite solution and 200 mL of 2M NaOH were added to the tube, followed by vigorous shaking until the adults broke open and embryos were released. The embryos were next washed for a total of 5 times by being suspended in 15mL M9, centrifuged, and had the supernatant removed. After the last wash, the embryos were resuspended in a final volume of 5mL of M9 and subsequently placed on a rotator at 20°C for 16-24h for synchronized L1 population to hatch. These animals were then grown until the L4 stage for imaging, with specific *E. coli* strains and plate types as described for each experiment.

Cross/strain construction and genotyping

Backcrosses were performed by crossing the animals with the allele of interest with N2 males. Male stocks were generated by preparing at least four 6cm NGM + OP50-1 plates with 10X L4 hermaphrodites with genotype of interest. The animals were heat-shock at 30°C for 6 hours and returned to 20°C for 48 hours before screening for males. Male stocks were propagated by plating excess males (~10-15) with a few L4 hermaphrodites (~2-3) on NGM + OP50-1 plates. Cross progeny were genotyped via PCR using worm lysates generated by single

worm lysis. Strain received from outside lab/sources or generated from CRISPR-Cas9-mediated genome editing were backcrossed at least 3 times while selecting for the allele of interest before analysis.

Worm strain generation was performed by generating male population of one of the genotypes of interest, or of the genotype with a fluorescent marker if applicable for easier identification of cross progenies. PCR was used to genotype for both genotypes of interests for each cross generation until both genotypes were identified to be homozygous. Or if one of the parental strains carry a fluorescence marker, homozygosity of that genotype was identified by confirming 100% of the progenies carry the fluorescence marker using the fluorescent dissecting microscope.

A complete list of worm strains used, and crosses performed to generate the worm strains can be found in Table 1.

A complete list of primers used can be found in Table 2.

RNAi interference experiments

RNAi interference experiments were performed via the feeding method. RNAi clones were streaked onto LB + carbenicillin (no Tetracycline) plates and grown overnight at 37°C. Then single colonies were picked into 4 mL LB + carbenicillin (25 mg/mL, for a final carbenicillin concentration of 25 μg/mL) solution and grown in a shaking incubator at 37°C for approximately 15.5 hours for all RNAi experiments included in Results or at 30°C for 16 hours for Appendix B. The overnight (R)OP50 bacterial culture was then plated onto RNAi plates (NGM plates supplemented with 5 mM isopropyl β-d-1-thiogalactopyranoside [IPTG], 1 mM carbenicillin), dried at room temperature, and incubated at 23°C for 3 days in dark. Gravid adult

animals are then added onto the plates for F1 progeny to be collected at L4 onto separate RNAi plates for thermotolerance assays or for fluorescence intensity quantification (Figure 4A & B, 7B & C)

Thermotolerance assays

Gravid adults were plated onto 6 cm NGM + OP50-1 plates (Figure 5C) or 6 cm RNAi plates seeded with overnight (R)OP50 culture (Figure 4C, 5D, 6C & D, 8; note: L4440 (OP50) bacteria is used for experiments without RNAi treatments) and grown at 20°C. After three days, L4 progeny were picked from a mixed population onto fresh 6 cm NGM + OP50-1 plates or corresponding seeded 6 cm RNAi plates. Three plates were prepared for each condition per experiment, and 30 L4s were plated per plate. The L4 animals were then subjected to heat shock in a dry programmable incubator at 37.5°C. The heat shock treatment started with a 15min gradual ramp up from 25°C to 37.5°C, and the temperature is held stable at 37.5°C for different durations: 1h 45 min (Figure 5D, 6C), 1h 55 min (Figure 6D), and 2h (Figure 4C, 5C, 8). 1h 45 min heat shock is typically used to accommodate the increase heat shock susceptibility of HSP-90::RFP^{int-OE} animals, and 2h heat shock is typically used for strain backgrounds other than HSP-90::RFP^{int-OE}. 1h 55 min heat shock was used in this study due to ongoing mechanical issues with the dry programmable incubator in use for heat shock that appear to have reduced heat shock efficacy at the time of experiments in Figure 6D resulting in lack of separation between susceptible vs non-susceptible phenotypes of controls, hence the adjustment from the original 1h 45 min to 1h 55 min was done as part of troubleshooting. Immediately following the heat shock at 37.5°C, the plates were removed from the incubator and laid out on benchtop in a single layer for cool down at room temperature for 30 min. The plates are then transferred to a 20°C

incubator for 24h prior to scoring for fraction of survival. Animals are scored in a blinded manner and those showing no movement upon a single poke were counted as dead. For each experiment, three independent replicates were performed on different days, with three plates scored per condition, 30 animals per plate, except as noted for Figure 5D.

CRISPR/Cas9

A co-CRISPR strategy was used to delete the *fbxa-11* coding region, using *gcy-8p::GFP* as the co-injection marker. Single guide RNA (sgRNA) was designed using the CRISPR design tool in Benchling, the ChopChop software, and the custom CRISPR-Cas9 gRNA designed tool on IDT. The following sgRNA sequences were used: sgRNA1: 5' – AGGGTAAACGTAGAACAGCT – 3', sgRNA2: 5' – ATGTATAATGTAGTGTATAA - 3'.

To prepare the injection mix, 0.24 µL of each of the sgRNA of 0.4 µg/µL concentration was mixed with 0.9 µL tracrRNA, 0.5 µL of 40 µM IDT Cas9, and then incubated at 37°C for 10 minutes. After incubation, *gcy-8p::GFP* (final concentration of 20 ng/µL), and Bluescript filler DNA (final concentration of 80 ng/uL) were added. The injection mix was then centrifuged, and the supernatant was micro-injected into wild-type animals. The injected animals were grown at 20°C and screened for transgenic F1s with neuronal green fluorescence. Lines with transgenic F1s were genotyped via PCR to isolate heterozygous animals with the *fbxa-11* deletion. Animals homozygous for the *fbxa-11* deletion were then generated from these lines and confirmed with Sanger sequencing for the CRISPR deletion. The deletion positive line was named *jy194* and backcrossed 3 times to the N2 background before further assessment.

Fluorescence Microscopy

For HSP-90::RFP-expressing animals shown in Figure 7A and *hsp-90p::GFP*-expressing animals shown in Appendix A, animals were bleached to obtain synchronized L1 population as described above, and then grown on 10 cm L4440(OP50) seeded RNAi plates (Figure 7A) or NGM + OP50-1 plates (Appendix A) for 43-44 hours at 20°C to reach L4 life stage. The animals were then washed off in M9 + tween 20, centrifuged to remove supernatant, anesthetized with 100mM levamisole, and transferred into a 96-well plate with fresh 10mM levamisole in M9 + tween 20. Imaging was performed using the ImageXpress Nano using a 4x objective (Molecular Devices, LLC) and analyzed using the ImageJ program. The quantified fluorescence signal was corrected by the mean background fluorescence sampled from three adjacent background region. Quantification of fluorescent signal was restricted to the anterior intestine, defined for this study to be the beginning of the intestine to the midpoint of the vulva region (Bardan Sarmiento et al., 2024).

For HSP-90::RFP-expressing animals shown in Figure 4A & B, and Figure 7B & C, L4 animals were picked from a mixed population grown at 20°C on 6cm RNAi plates, mounted on 2% agarose pads while anesthetized with 100mM levamisole, and imaged with Zeiss Axioimager M1 compound microscope with a 10X objective. Whole animal fluorescent signal was analyzed using the ImageJ program. The quantified fluorescence signal was corrected by the mean background fluorescence sampled from three adjacent background regions.

APPENDICES

Figure A1: CUL-6 deletion increases *hsp-90* promoter activity.

Quantification of GFP signal in the anterior intestine of hsp-90p::GFP animals and hsp-90p::GFP animals with *cul-6(ok1614)* deletion and intestinal CUL-6 overexpression.
Experiment was performed in triplicate, each replicate performed on independent days. Each dot represents the GFP intensity of an animal. n = 155-161 animals were quantified.
Mean fraction alive of the triplicate is represented by black bar with error bars as SD. P-values were determined by A Mann-Whitney test. ****$p < 0.0001$

Figure A1

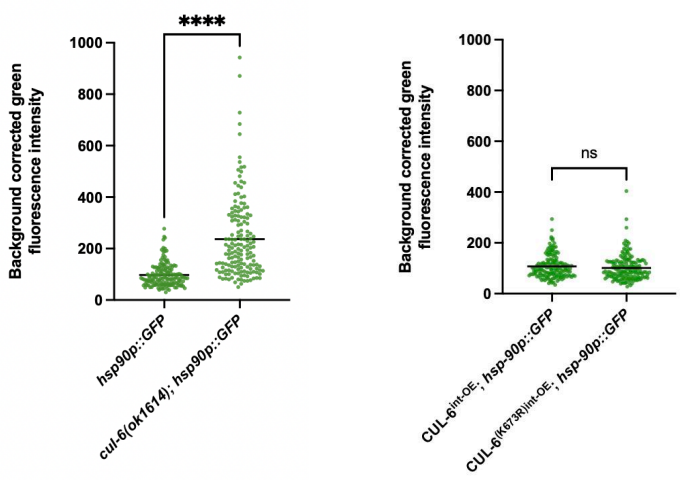
****
Background corrected green fluorescence intensity
1000
800
600
400
200
0
hsp90p::GFP
cul-6(ok1614); hsp90p::GFP
ns
Background corrected green fluorescence intensity
1000
800
600
400
200
0
CUL-6^(int-OE); hsp-90p::GFP
CUL-6^(K673R)int-OE; hsp-90p::GFP

We previously found that CUL-6/cullin ubiquitin ligase activity affects the level of HSP-90::RFP$^{int\text{-}OE}$ expression (here, HSP-90::RFP is overexpressed from the intestinal-specific *vha-6* promoter). Specifically, a *cul-6* deletion increases the level of HSP-90::RFP, while overexpression of wild-type, but not mutant CUL-6 lowers HSP-90::RFP levels (Bardan Sarmiento et al., 2024). However, whether CUL-6 activity regulates the endogenous *hsp-90* promoter (which was not used with the intestinal-specific HSP-90 overexpression experiments) was not known.

Taking an existing *hsp-90p:GFP* reporter strain where the endogenous *hsp-90* promoter is driving GFP expression, I backcrossed this extrachromosomal transgene arrays with wild-type N2 animals four times and crossed it with strains carrying different *cul-6* mutations: the *cul-6(ok1614)* deletion, CUL-6 overexpression, and neddylation-deficient CUL-6 overexpression. Images of GFP expression in L4 animals and GFP readout measurements were obtained via similar methods as used in Figure 7A. The GFP measurement comparisons were performed as followed: *hsp-90p::GFP* expression in a wild-type background was compared to *hsp-90p::GFP* expression in a *cul-6(ok1614)* deletion background. Separately, expression of *hsp-90p::GFP* in a wild-type CUL-6 overexpression background was compared to *hsp-90p::GFP* overexpression in a neddylation-deficient CUL-6 overexpression background. These comparisons were performed separately, because the CUL-6 overexpression transgene contains a C-terminal GFP (CUL-6::GFP) that might confound hsp-90p::GFP expression measurements, although CUL-6::GFP is at much lower levels than hsp-90p::GFP (not shown).

Here, I observed that *hsp-90::GFP* expression was significantly higher in *cul-6* mutants compared to wild-type animals. This effect potentially leads to higher levels of endogenous HSP-90 protein, and thus overall higher HSP-90 protein in the context of experiments performed with HSP-90 overexpression (Bardon Sarmiento et al., 2024). On the other hand, there was no significant difference observed between the GFP level of animals in the different CUL-6 overexpression backgrounds. This result suggest that CUL-6 overexpression does not impact *hsp-90* promoter activity.

Figure A2: Overnight cultures of (R)OP50 grown at 30°C have better efficacy at knockdown of *cul-6* and *hsp-90*.

1. Quantification of whole body GFP signal of CUL-6$^{int\text{-}OE}$ animals after being fed *(R)OP50* expressing empty vector or RNAi for *cul-6.*
2. Quantification of whole body RFP signal of HSP-90::RFP$^{int\text{-}OE}$ animals after being fed *(R)OP50* expressing empty vector or RNAi for *hsp-90.*

For 1-2, experiments were performed in duplicate, each replicate performed on independent days. Each dot represents the GFP or RFP intensity of an animal. n = 36-43 animals were quantified for A and n= 34-40 for B.
Mean fraction alive of the triplicate is represented by black bar with error bars as SD. P-values were determined by by Kruskal Wallis test with Dunn's multiple comparisons test. ***$p < 0.001$, and ****$p < 0.0001$.

Figure A2

1

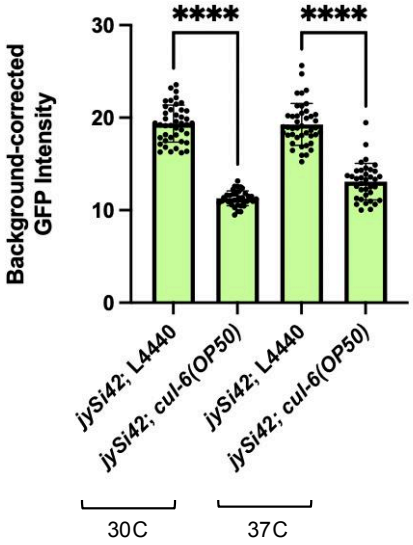
Background-corrected GFP Intensity
30
20
10
0
****
****
jySi42; L4440
jySi42; cul-6(OP50)
jySi42; L4440
jySi42; cul-6(OP50)
30C
37C

2

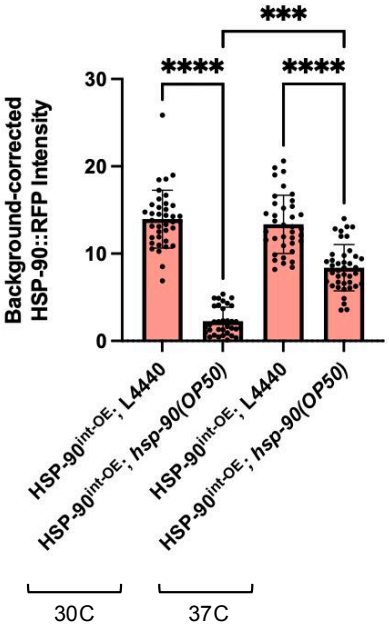
Background-corrected HSP-90::RFP Intensity
30
20
10
0
***
****
****
HSP-90int-OE; L4440
HSP-90int-OE; hsp-90(OP50)
HSP-90int-OE; L4440
HSP-90int-OE; hsp-90(OP50)
30C
37C

In an attempt to optimize the efficacy of RNAi knockdown by the bacteria feeding method (Conte et al., 2015), I tested different inoculation temperatures for growing bacterial overnight cultures. Different growing temperatures could impose different selective pressures on bacteria and therefore could have implications on the loss or persistence of dsRNA-producing plasmid, because carrying a plasmid can inflict a fitness cost (Ponciano et al., 2007). A past report found that RNAi potency seems to be linked with the concentration of dsRNA fed to the animals (Rea et al., 2007; Zhuang & Hunter, 2011), therefore the impact of growing temperatures on RNAi potency warrants assessment. In particular, I pursued this angle of investigation due to several of my experiments where *cul-6* RNAi failed to generate known phenotypes, such as lowering of thermotolerance.

I tested two different growing temperatures for the duration of 16 hours: 30°C and 37°C. The RNAi clones I tested were *cul-6(OP50)* and *hsp-90(OP50)*, which are key reagents used for thermotolerance experiments described above (Bardan Sarmiento et al., 2024; Panek et al., 2020). We have transgenic strains carrying fluorescent markers for CUL-6 and HSP-90, making the assessment of the RNAi potency quantifiable with fluorescence intensity as a convenient readout: CUL-6$^{int\text{-}OE}$ animals overexpress CUL-6 tagged with GFP, while HSP-90::RFP$^{int\text{-}OE}$ animals overexpress HSP-90 tagged with RFP. For *cul-6(OP50)* RNAi, incubating at 30°C marginally improved RNAi knockdown efficacy compared to incubating at 37°C. For *hsp-90(OP50)* RNAi, incubating at 30°C significantly improved knockdown efficacy of HSP-90::RFP expression, as shown by the significantly lower HSP-90::RFP following RNAi treatment compared to treating with bacteria incubated at 37°C. Some limitations of this set up include that the agar plates used to streak out RNAi clones contained only LB and carbenicillin

but no tetracycline. OD600 was also not measured for this study and could be investigated to further understand the relationship between optimal bacteria growth phase and RNAi potency. Regardless, this assessment between bacteria incubated at two different temperatures indicated that incubation at 30°C has the potential to achieve higher knockdown efficacy.

REFERENCES

Aviner, R., & Frydman, J. (2020). Proteostasis in Viral Infection: Unfolding the Complex Virus–Chaperone Interplay. *Cold Spring Harbor Perspectives in Biology*, *12*(3), a034090. https://doi.org/10.1101/cshperspect.a034090

Bakowski, M. A., Desjardins, C. A., Smelkinson, M. G., Dunbar, T. A., Lopez-Moyado, I. F., Rifkin, S. A., Cuomo, C. A., & Troemel, E. R. (2014). Ubiquitin-Mediated Response to Microsporidia and Virus Infection in C. elegans. *PLOS Pathogens*, *10*(6), e1004200. https://doi.org/10.1371/journal.ppat.1004200

Balla, K. M., Lažetić, V., & Troemel, E. R. (2019). Natural variation in the roles of C. elegans autophagy components during microsporidia infection. *PLOS ONE*, *14*(4), e0216011. https://doi.org/10.1371/journal.pone.0216011

Bardan Sarmiento, M., Gang, S. S., Oosten-Hawle, P. van, & Troemel, E. R. (2024). CUL-6/cullin ubiquitin ligase-mediated degradation of HSP-90 by intestinal lysosomes promotes thermotolerance. *Cell Reports*, *43*(6). https://doi.org/10.1016/j.celrep.2024.114279

Bonthala, V. S., & Stich, B. (2022). Genetic Divergence of Lineage-Specific Tandemly Duplicated Gene Clusters in Four Diploid Potato Genotypes. *Frontiers in Plant Science*, *13*. https://doi.org/10.3389/fpls.2022.875202

Ciechanover, A. (1998). The ubiquitin–proteasome pathway: On protein death and cell life. *The EMBO Journal*, *17*(24), 7151–7160. https://doi.org/10.1093/emboj/17.24.7151

Conte, D., MacNeil, L. T., Walhout, A. J. M., & Mello, C. C. (2015). RNA Interference in Caenorhabditis Elegans. *Current Protocols in Molecular Biology*, *109*, 26.3.1-26.330. https://doi.org/10.1002/0471142727.mb2603s109

Duda, D. M., Borg, L. A., Scott, D. C., Hunt, H. W., Hammel, M., & Schulman, B. A. (2008). Structural Insights into NEDD8 Activation of Cullin-RING Ligases: Conformational Control of Conjugation. *Cell*, *134*(6), 995–1006. https://doi.org/10.1016/j.cell.2008.07.022

El-Brolosy, M. A., & Stainier, D. Y. R. (2017). Genetic compensation: A phenomenon in search of mechanisms. *PLoS Genetics*, *13*(7), e1006780. https://doi.org/10.1371/journal.pgen.1006780

Ellis, R. J., & Vies, S. M. van der. (1991). MOLECULAR CHAPERONES. *Annual Review of Biochemistry*, *60*(Volume 60, 1991), 321–347. https://doi.org/10.1146/annurev.bi.60.070191.001541

Ho Zhi Guang, M., Kavanagh, E. L., Dunne, L. P., Dowling, P., Zhang, L., Lindsay, S., Bazou, D., Goh, C. Y., Hanley, C., Bianchi, G., Anderson, K. C., O'Gorman, P., & McCann, A. (2019). Targeting Proteotoxic Stress in Cancer: A Review of the Role that Protein

Quality Control Pathways Play in Oncogenesis. *Cancers*, *11*(1), Article 1. https://doi.org/10.3390/cancers11010066

Iconomou, M., & Saunders, D. N. (2016). Systematic approaches to identify E3 ligase substrates. *Biochemical Journal*, *473*(22), 4083–4101. https://doi.org/10.1042/BCJ20160719

Jin, J., Ang, X. L., Shirogane, T., & Wade Harper, J. (2005). Identification of Substrates for F-Box Proteins. In *Methods in Enzymology* (Vol. 399, pp. 287–309). Academic Press. https://doi.org/10.1016/S0076-6879(05)99020-4

Kettern, N., Dreiseidler, M., Tawo, R., & Höhfeld, J. (2010). Chaperone-assisted degradation: Multiple paths to destruction. *Biological Chemistry*, *391*(5), 481–489. https://doi.org/10.1515/bc.2010.058

Kobayashi, Y., Tian, S., & Ui-Tei, K. (2022). The siRNA Off-Target Effect Is Determined by Base-Pairing Stabilities of Two Different Regions with Opposite Effects. *Genes*, *13*(2), Article 2. https://doi.org/10.3390/genes13020319

Kuo, C.-J., Hansen, M., & Troemel, E. (2018). Autophagy and innate immunity: Insights from invertebrate model organisms. *Autophagy*, *14*(2), 233–242. https://doi.org/10.1080/15548627.2017.1389824

Lažetić, V. (2020). Conservation lost: Host-pathogen battles drive diversification and expansion of gene families. *The FEBS Journal*, *288*(18), 5289–5299. https://doi.org/10.1111/febs.15627

Ma, F., Lau, C. Y., & Zheng, C. (2021). Large Genetic Diversity and Strong Positive Selection in F-Box and GPCR Genes among the Wild Isolates of Caenorhabditis elegans. *Genome Biology and Evolution*, *13*(5), evab048. https://doi.org/10.1093/gbe/evab048

Martinez, M. A. Q., & Matus, D. Q. (2020). Auxin-mediated Protein Degradation in Caenorhabditis elegans. *Bio-Protocol*, *10*(8), e3589. https://doi.org/10.21769/BioProtoc.3589

Mello-Vieira, J., Bopp, T., & Dikic, I. (2023). Ubiquitination and cell-autonomous immunity. *Current Opinion in Immunology*, *84*, 102368. https://doi.org/10.1016/j.coi.2023.102368

Mocellin, S., & Provenzano, M. (2004). RNA interference: Learning gene knock-down from cell physiology. *Journal of Translational Medicine*, *2*, 39. https://doi.org/10.1186/1479-5876-2-39

Morimoto, R. I. (2008). Proteotoxic stress and inducible chaperone networks in neurodegenerative disease and aging. *Genes & Development*, *22*(11), 1427–1438. https://doi.org/10.1101/gad.1657108

Onchuru, T. O., & Kaltenpoth, M. (2019). Quantitative PCR primer design affects quantification of dsRNA-mediated gene knockdown. *Ecology and Evolution*, *9*(14), 8187–8192. https://doi.org/10.1002/ece3.5387

Panek, J., Gang, S. S., Reddy, K. C., Luallen, R. J., Fulzele, A., Bennett, E. J., & Troemel, E. R. (2020). A cullin-RING ubiquitin ligase promotes thermotolerance as part of the intracellular pathogen response in Caenorhabditis elegans. *Proceedings of the National Academy of Sciences*, *117*(14), 7950–7960. https://doi.org/10.1073/pnas.1918417117

Ponciano, J. M., De Gelder, L., Top, E. M., & Joyce, P. (2007). The Population Biology of Bacterial Plasmids: A Hidden Markov Model Approach. *Genetics*, *176*(2), 957–968. https://doi.org/10.1534/genetics.106.061937

Rea, S. L., Ventura, N., & Johnson, T. E. (2007). Relationship Between Mitochondrial Electron Transport Chain Dysfunction, Development, and Life Extension in Caenorhabditis elegans. *PLOS Biology*, *5*(10), e259. https://doi.org/10.1371/journal.pbio.0050259

Reddy, K. C., Dror, T., Sowa, J. N., Panek, J., Chen, K., Lim, E. S., Wang, D., & Troemel, E. R. (2017). An Intracellular Pathogen Response Pathway Promotes Proteostasis in C. elegans. *Current Biology*, *27*(22), 3544-3553.e5. https://doi.org/10.1016/j.cub.2017.10.009

Reddy, K. C., Dror, T., Underwood, R. S., Osman, G. A., Elder, C. R., Desjardins, C. A., Cuomo, C. A., Barkoulas, M., & Troemel, E. R. (2019). Antagonistic paralogs control a switch between growth and pathogen resistance in C. elegans. *PLOS Pathogens*, *15*(1), e1007528. https://doi.org/10.1371/journal.ppat.1007528

Ruano, D. (2021). Proteostasis Dysfunction in Aged Mammalian Cells. The Stressful Role of Inflammation. *Frontiers in Molecular Biosciences*, *8*. https://doi.org/10.3389/fmolb.2021.658742

Schopf, F. H., Biebl, M. M., & Buchner, J. (2017). The HSP90 chaperone machinery. *Nature Reviews Molecular Cell Biology*, *18*(6), 345–360. https://doi.org/10.1038/nrm.2017.20

Shmidt, T., Hampich, F., Ridders, M., Schultrich, S., Hans, V. H., Tenner, K., Vilianovich, L., Qadri, F., Alenina, N., Hartmann, E., Köhler, M., & Bader, M. (2007). Normal brain development in importin-α5 deficient-mice. *Nature Cell Biology*, *9*(12), 1337–1338. https://doi.org/10.1038/ncb1207-1337

Thomas, J. H. (2006). Adaptive evolution in two large families of ubiquitin-ligase adapters in nematodes and plants. *Genome Research*, *16*(8), 1017–1030. https://doi.org/10.1101/gr.5089806

To, P., Xia, Y., Lee, S. O., Devlin, T., Fleming, K. G., & Fried, S. D. (2022). A proteome-wide map of chaperone-assisted protein refolding in a cytosol-like milieu. *Proceedings of the National Academy of Sciences of the United States of America*, *119*(48), e2210536119. https://doi.org/10.1073/pnas.2210536119

Wang, A., Chen, W., & Tao, S. (2021). Genome-wide characterization, evolution, structure, and expression analysis of the F-box genes in Caenorhabditis. *BMC Genomics*, *22*(1), 889. https://doi.org/10.1186/s12864-021-08189-7

Willis, M. S., & Patterson, C. (2013). Proteotoxicity and Cardiac Dysfunction—Alzheimer's Disease of the Heart? *New England Journal of Medicine*, *368*(5), 455–464. https://doi.org/10.1056/NEJMra1106180

Yamazaki, Y., Akashi, R., Banno, Y., Endo, T., Ezura, H., Fukami-Kobayashi, K., Inaba, K., Isa, T., Kamei, K., Kasai, F., Kobayashi, M., Kurata, N., Kusaba, M., Matuzawa, T., Mitani, S., Nakamura, T., Nakamura, Y., Nakatsuji, N., Naruse, K., Niki, H., Nitasaka, E., Obata, Y., Okamoto, H., Okuma, M., Sato, K., Serikawa, T., Shiroishi, T., Sugawara, H., Urushibara, H., Yamamoto, M., Yaoita, Y., Yoshiki, A., Kohara, Y. (2010). NBRP databases: Databases of biological resources in Japan. *Nucleic Acids Research*, *38*(suppl_1), D26–D32. https://doi.org/10.1093/nar/gkp996

Yen, H.-C. S., & Elledge, S. J. (2008). Identification of SCF Ubiquitin Ligase Substrates by Global Protein Stability Profiling. *Science*, *322*(5903), 923–929. https://doi.org/10.1126/science.1160462

Yoshida, Y., Saeki, Y., Murakami, A., Kawawaki, J., Tsuchiya, H., Yoshihara, H., Shindo, M., & Tanaka, K. (2015). A comprehensive method for detecting ubiquitinated substrates using TR-TUBE. *Proceedings of the National Academy of Sciences*, *112*(15), 4630–4635. https://doi.org/10.1073/pnas.1422313112

Zhang, L., Ward, J. D., Cheng, Z., & Dernburg, A. F. (2015). The auxin-inducible degradation (AID) system enables versatile conditional protein depletion in C. elegans. *Development*, *142*(24), 4374–4384. https://doi.org/10.1242/dev.129635

Zhuang, J. J., & Hunter, C. P. (2011). Tissue Specificity of Caenorhabditis elegans Enhanced RNA Interference Mutants. *Genetics*, *188*(1), 235–237. https://doi.org/10.1534/genetics.111.127209